Development of versatile allele-specific siRNAs able to silence all the dominant dynamin 2 mutations

Swati Dudhal, Lylia Mekzine, Bernard Prudhon, Karishma Soocheta, Bruno Cadot, Kamel Mamchaoui, Delphine Trochet, Marc Bitoun

Development of versatile allele-specific siRNAs able to silence all the dominant Dynamin 2 mutations

Swati Dudhal[1*], Lylia Mekzine[1*], Bernard Prudhon[1], Karishma Soocheta[1], Bruno Cadot[1], Kamel Mamchaoui[1], Delphine Trochet[1†,] Marc Bitoun[1†]

*: co-first authors. †: co-last authors.

1. Sorbonne Université, Inserm, Institut de Myologie, Centre de Recherche en Myologie, F-75013 Paris, France.

*Corresponding authors: Delphine Trochet (d.trochet@institut-myologie.org) or Marc Bitoun (m.bitoun@institut-myologie.org), Centre de Recherche en Myologie, UMRS 974, Institut de Myologie, Paris, France. Tel: 33 (0) 1.42.16.57.18. Fax: 33 (0) 1.42.16.57.00.

Running title: Allele-specific silencing of dominant *DNM2* mutations

Abstract

Dominant centronuclear myopathy (CNM) is a rare form of congenital myopathy associated with a wide clinical spectrum, from severe neonatal to milder adult forms. There is no available treatment for this disease due to heterozygous mutations in the *DNM2* gene encoding Dynamin 2 (DNM2). Dominant *DNM2* mutations also cause rare forms of Charcot-Mare-Tooth disease and hereditary spastic paraplegia and deleterious DNM2 overexpression was noticed in several diseases. The proof of concept for therapy by allele-specific RNA interference devoted to silence the mutated mRNA without affecting the normal allele was previously achieved in a mouse model and patient-derived cells, both expressing the most frequent *DNM2* mutation in CNM. In order to have versatile siRNAs usable regardless of the mutation, we have developed allele-specific siRNAs against 2 non-pathogenic single nucleotide polymorphisms (SNP) frequently heterozygous in the population. In addition, allele-specific siRNA against the p.S619L DNM2 mutation, a mutation frequently associated with severe neonatal cases, were developed. The beneficial effects of these new siRNAs are reported for a panel of defects occurring in patient-derived cell lines. The development of these new molecules allows targeting the large majority of the patients harbouring *DNM2* mutations or overexpression by only a few siRNA.

Introduction

Autosomal dominant centronuclear myopathy (AD-CNM, MIM #160150) is a rare congenital myopathy associated with a wide clinical spectrum from severe-neonatal to mild-adult forms [1]. The classical late-childhood or adult-onset form exhibits delayed motor milestones and diffuse skeletal muscle weakness mainly involving facial and limb muscles whereas paediatric patients affected by the severe neonatal form usually have generalized weakness, hypotonia, and facial weakness [2,3]. AD-CNM results from mutations in the *DNM2* gene which encodes dynamin 2 (DNM2) [4]. In addition, *DNM2* mutations also cause rare forms of Charcot-Marie-Tooth disease (CMT) [5] and hereditary spastic paraplegia (HSP) [6] and a deleterious DNM2 overexpression was reported in several cancers [7–12] and the X-linked recessive CNM [13], highlighting a large DNM2 involvement in human diseases. DNM2 belongs to the superfamily of large GTPases [14] acting as a mechanochemical scaffolding molecule that oligomerizes and deforms biological membranes leading to the formation and release of vesicles from the plasma membrane and intracellular membrane compartments. Furthermore, several studies have highlighted the role of DNM2 as a regulator of both actin and microtubule cytoskeletons [15,16]. More than 30 *DNM2* mutations have been reported in AD-CNM patients [17] and, when tested, the mutant protein is normally expressed [4,18]. Mutations are thought to be responsible for a gain of function and/or a dominant-negative effect through an increased GTPase activity and formation of abnormal stable DNM2 oligomers [19,20]. In addition, absence of haploinsufficiency in AD-CNM is supported by data from patients and absence of phenotype developed by heterozygous knockout mice expressing 50% Dnm2 [13,21].

We recently developed a therapeutic approach for the *DNM2*-related AD-CNM by allele-specific RNA interference (AS-RNAi) devoted to specifically suppressing the expression of the mutated protein from the mutated allele without reducing expression from the wild-type allele

[22]. AS-RNAi was demonstrated as a powerful strategy in cells from patients and animal models of numerous dominant inherited diseases [23] and led to two clinical trials targeting a Keratin 6a mutation causing Pachyonychia congenita [24] and one mutation of the *KRAS* gene involved in pancreatic cancer [25]. By applying this strategy, we reported functional rescue in the Knock-In-*Dnm2*$^{R465W/+}$ mouse model of AD-CNM and patient-derived fibroblasts, both expressing the most frequent mutation encountered in patients (p.R465W found in around 30% of patients) [22]. Extending this strategy to the entire AD-CNM patient population requires either to develop personalized medicine through specific siRNA for each reported mutation or to develop an alternative approach allowing to target the distinct dominant *DNM2* mutations using a limited number of allele-specific siRNA. In particular cases of triplet repeat diseases such as Huntington's disease or spinocerebellar ataxia in which the sequence of the genetic mutations makes allele-specific silencing challenging, AS-siRNA have been developed against disease-associated single nucleotide polymorphisms (SNP) [23,26–28]. We took advantage of the presence in the *DNM2* sequence of two non-pathogenic SNPs frequently heterozygous in the general population to develop a similar strategy for the AD-CNM. Here, we report the identification of effective AS-siRNA against the two nucleotide versions of the two non-pathogenic DNM2 SNPs which may be used to silence any mutation carried by the same mRNA. In addition, the first AS-siRNAs targeting a *DNM2* mutation associated with severe neonatal phenotype, i.e. the p.S619L mutation, have been developed. We also report the functional benefits of this new set of siRNAs on several defects identified in patient-derived cell lines. The development of these new AS-siRNA, in addition to the previous ones against the p.R465W mutation, provides a panoply of allele-specific molecules able to target the large majority of AD-CNM patients. Interestingly, siRNAs against the DNM2 SNPs represent versatile molecules with larger potential applications to silence *DNM2* mutations in CMT and HSP and to reduce DNM2 expression in a controlled manner in diseases associated with deleterious overexpression.

92

Results

Identification of targetable SNPs and heterozygous cells

We performed an *in-silico* analysis devoted to identifying DNM2 SNPs exhibiting the highest frequency of heterozygosity in Human. We looked in Ensembl Genome Browser (https://www.ensembl.org - human genome assembly GRCh38.p13) for synonymous variants in the *DNM2* open reading frame or variants in the 5'- and 3'-untranslated transcribed regions (UTR) exhibiting a frequency of the second most common allele between 0.1 and 0.5 in the general population. Using these criteria, we identified two SNPs (Figure 1A). The first SNP was a T/C variation (rs2229920, thereafter called SNP1) identified as a synonymous variant of the Alanine 713 (c.2139T>C, NM_001005361.3) of the DNM2 protein. Allele frequencies for SNP1 were determined at 0.688 for the allele T and 0.321 for the allele C on 250 390 counts (gnomAD exomes r2.1.1) resulting in a theorical heterozygous (HTZ) frequency of 0.43 (calculated as 2 x frequency of T allele x frequency of C allele). In agreement, PCR and Sanger sequencing in a cohort of 52 CNM patients identified 42.3% of SNP1 heterozygosity. The second SNP was an A/T variation (rs12461992, thereafter called SNP2) identified as a 3'-UTR variant located 268 nucleotides after the stop codon (*268A>T, NM_001005361.3). Allele frequencies for SNP2 were determined at 0.824 for the allele A and 0.176 for the allele T resulting in a theorical HTZ frequency of 0.29 on 143 008 counts (gnomAD exomes r3.0) and 23% of SNP2 heterozygosity was found in our cohort of patient. No clinical sign was associated with SNP1 and SNP2.

We next thought to identify cells harbouring the SNPs at HTZ state which were required to screen for allele-specific siRNA against the SNPs. RT-PCR products encompassing the SNPs were amplified from fibroblast cell lines from 2 healthy controls and 2 CNM patients. Sanger sequencing of these RT-PCR products led to identifying one healthy control cell line

heterozygous for the 2 SNPs, one CNM cell line (p.R522H DNM2 mutation) harbouring the 2 SNPs at HTZ state, and one CNM cell line (p.S619L DNM2 mutation) harbouring only the SNP1 at HTZ state (Figure 1B). Through RT-PCR, cloning, and Sanger sequencing of a single allele, we determined that in the R522H cell line, the mutated mRNA also harboured the C version of SNP1 and T version of SNP2 and that in the S619L cell line, the mutated mRNA harboured the C version of SNP1 (Figure 1C). Altogether, we identified 2 SNPs targetable by AS-RNAi, one healthy control cell line to perform the siRNA screening, and 2 patient-derived cell lines for the functional evaluation of the identified AS-siRNA.

Allele-specific siRNA against the C allele of SNP1

For all the screening for allele-specific siRNA against SNP1 and SNP2 reported in this study, we used one healthy control cell line and looked for allele-specific siRNA leading to around 50% expression of DNM2 mRNA and protein due to specific silencing of the targeted allele. We first thought to identify AS-siRNA against the C version of the SNP1 (Figure 2 and Supp. Figure 1). Twelve 19-nucleotide siRNA carrying a single mismatch with the untargeted T version on the positions 5 to 17 (called si5 to si17) were assessed. At low concentration (30 nM), si6 and si11 were not able to significantly reduce *DNM2* mRNA expression compared to scramble siRNA-transfected cells (Figure 2A). In addition, si5, si13, and si14 led to an excessive reduction of *DNM2* transcript relative to the expected 50% and 7 siRNAs (si7, si8, si9, si10, si12, si15, and si17) reduced the *DNM2* expression in the expected range (Figure 2A). RT-PCR and BglI restriction enzyme digestion assay was used to discriminate the C (digested) from the T (undigested) alleles of SNP1 (Supp Figure 2A). The 7 siRNA reduced the C/T ratio compared to scramble siRNA (Figure 2B) with the lower ratio reached by si8 and si9. Quantification of each allele relative to *HPRT* mRNA showed that si8, si9, and si10 reduced expression of the allele C without affecting the T (Supp Figure 1A). At the same concentration,

si8, si9, and si10 also reduced expression of the DNM2 protein around the expected 50% compared to scramble siRNA in western blot (Supp Figure 1B). The maintenance of allele-specificity at higher concentration (100nM) was then assessed for si8, si9, and si10. The 3 siRNA reduced total *DNM2* mRNA content, and close to the expected 50% decrease for si8 and si9 (Figure 2C). Allele-specificity of si8 and si9 against the targeted C allele was maintained as demonstrated by the C/T ratio reduction (Figure 2D) and confirmed by quantification of each allele relative to *HPRT* expression (Supp Figure 1C). Maintenance of efficacy and allele-specificity of si8 and si9 at higher concentration was also demonstrated on DNM2 protein by western blot showing a significant decrease in DNM2 protein content which did not exceed 50% (Figure 2E). Altogether, these data validate si8 and si9 as the best allele-specific siRNA against the C version of the SNP1.

Allele-specific siRNA against the T allele of the SNP1

To identify AS-siRNA against the T version of SNP1, we assessed siRNA with mismatches at positions 8, 9, and 10, relative to the untargeted C allele in agreement with our previous screening. At low concentration (30 nM), si8 and si9 significantly reduced the *DNM2* expression in the expected range (Figure 3A). The RT-PCR assay and BglI digestion used to distinguish the targeted T allele from the untargeted C allele showed that the 3 siRNA significantly reduced the T/C ratio compared to scramble siRNA (Figure 3B, Supp Figure 3A). Of note, an increase in the untargeted allele C was observed with si9 (Supp Figure 3A, right panel) suggestive of a genetic regulation promoting the expression of the untargeted allele. At this concentration, the DNM2 protein content was not changed with these 3 siRNA (Supp Figure 3B). At higher concentration (100nM), total *DNM2* mRNA amount was reduced for the 3 siRNAs remaining close to the 50% threshold for si8 and si9 (Figure 3C), and allele-specificity of the 3 siRNAs against the targeted T allele was maintained as demonstrated by the

T/C ratio reduction (Figure 3D) and the quantification of each allele relative to *HPRT* expression (Supp Figure 3C). A significant increase in the untargeted allele was still observed (Supp Figure 3C, right panel) for the si9 and si10. At this concentration, western blot showed a significant decrease in DNM2 protein content for the si8, si9, and si10 compared to scramble siRNA (Figure 3E). Altogether, these data validate si8 and si9 as allele-specific siRNAs against the T version of the SNP1.

Allele-specific siRNA against the T allele of the SNP2

To screen for AS-siRNA against the T version of SNP2, twelve siRNA carrying a mismatch with the untargeted A allele from positions 6 to 17 were assessed (Figure 4 and Supp Figure 4). Transfected at 30 nM for 48h, si11, si12, si13, si14, si15, si16, and si17 reduced *DNM2* mRNA expression compared to scramble siRNA-transfected cells, and with the exception of si14 and si15 they all led to a reduction close to 50% (Figure 4A). RT-PCR and Psp5II restriction enzyme digestion assay was used to discriminate the T digested allele from the A undigested allele (Figure 4B, Supp Figure 1). Using this assay, we showed that the lower T/A ratio compared to scramble siRNA was reached by si11, si16, and si17 (Figure 4B). Quantification of each allele relative to *HPRT* mRNA showed that reduced T/A ratio resulted from a decrease in the expression of the T allele without reducing the A (Supp Figure 4A). For si17, a significant increase in the A allele was also noticed (Supp Figure 4A, right panel). At this low concentration, only si11 and si16 reduced expression of the DNM2 protein around the expected 50% when compared to scramble siRNA (Supp Figure 4B). We next assessed the maintenance of allele-specificity for si11, si16, and si17 at higher concentration (100nM). Semi-quantitative RT-PCR showed a significant reduction of around 50% of total *DNM2* mRNA for each siRNA (Figure 4C). The 3 siRNA reduced the T/A ratio compared to scramble siRNA (Figure 4D) through a specific impact on the T allele for si11 and si16 (Supp Figure 4C). At this higher

concentration, DNM2 protein content did not exceed 50% (Figure 4E). Altogether, these data validate si11 and si16 as efficient allele-specific siRNA against the T version of the SNP2.

Allele-specific siRNA against the A allele of SNP2

Previous results on the T allele of SNP2 showed a large number of mismatch positions in the siRNAs efficient to develop AS-siRNA. Consequently, we started the screening for AS-siRNA against the A allele by introducing one mismatch in the central region of the siRNA (positions 9, 10, and 11) frequently showed with the highest specificity in previously reported studies (Figure 5 and Supp Figure 5) [23]. At low concentration (30 nM), si9, si10, and si11 significantly reduced the DNM2 expression in the expected 50% range (Figure 5A). The RT-PCR assay and Psp5II digestion used to distinguish the targeted A allele from the untargeted T allele showed that the 3 siRNA significantly reduced the A/T ratio compared to scramble siRNA through the highest impact on the A allele for si9 and si11 (Figure 5B and Supp Figure 5A). At this concentration, the DNM2 protein content was significantly reduced with si10 and si11 (Supp Figure 5B). At higher concentration (100nM), a significant reduction of total *DNM2* mRNA was observed for the 3 siRNAs (Figure 5C) and Psp5II digestion of the RT-PCR products showed maintenance of allele-specificity (Figure 5D). Quantification of each allele relative to *HPRT* expression showed a reduction of the A allele using si9 and si11 and an upregulation of the untargeted allele T with the 3 siRNA (Supp Figure 5C). At this concentration, DNM2 protein content, quantified by western blot, was reduced by si10 and si11 (Figure 5E) but not by si9 probably due to the upregulation of the untargeted T allele (Supp Figure 5C). Altogether, these data validate si11 as the most efficient allele-specific siRNA against the A version of the SNP2.

Allele-specific siRNA against the p.S619L DNM2 mutation

In order to compare the functional benefit of siRNA directed against the SNPs or a mutation, we screened for AS-siRNA against the p.S619L (c.C1856T) (Figure 6 and Supp Figure 6). The S619L patient-derived fibroblasts were used to screen for 15 siRNA (si3 to si17) named depending on the position of the mismatch with the wild-type (WT) sequence of the *DNM2* mRNA. At low concentration (30 nM), si9 and si11 were not able to significantly reduce *DNM2* mRNA expression compared to scramble siRNA and si4, si5, si7 and si16 led to an excessive reduction of *DNM2* transcript relative to the 50% expected (Figure 6A). Nine siRNAs (si3, si6, si8, si10, si12, si13, si14, si15, and si17) significantly reduced the *DNM2* expression, and among them, the si6, si8, si10, si13, si15, si17 reduced mRNA amount in the expected range around 50% (Figure 6A). Given that the S619L mutation does not introduce or remove a restriction site relative to the WT sequence, we used the presence of the SNP1 at the heterozygous state in this patient cell line to quantify allele-specificity of the 9 siRNAs using BglI digestion of the SNP1 sequence (the C allele of SNP1 and the DNM2 mutation carried by the same mRNA, Figure 1C and Supp Figure 7B). The 9 siRNA significantly reduced the C/T (i.e. the mutant/WT) ratio compared to scramble siRNA (Figure 6B) with the lower ratio reached by si10. Quantification of each allele relative to *HPRT* mRNA showed that the 9 siRNAs reduced expression of the mutated allele with some of them inducing increased in the WT allele (Supp Figure 6A). We assessed the impact on the DNM2 protein content of 4 siRNAs out of the 15 (si6, si8, si10, and si13) and showed a significant reduction which did not exceed 50% for the 4 siRNAs (Supp Figure 6B). At higher concentration (100 nM), a significant reduction of total *DNM2* mRNA was observed for the 4 siRNA (Figure 6C) and allele-specificity was maintained (Figure 6D and Supp Figure 6C) with the maximum impact on the mutated mRNA reached with the si10. At this concentration, DNM2 protein content, quantified by western blot, was significantly reduced by the 4 siRNAs and the decrease did not exceed

50% (Figure 6E). Altogether, these data validate 4 allele-specific siRNA (si6, si8, si10 and si13) against the S619L DNM2 mutant allele.

Rescue of clathrin-mediated endocytosis and cell surface by AS-siRNA

DNM2 is well recognized for its role in endocytosis and the defect of clathrin-mediated endocytosis (CME) was previously demonstrated in AD-CNM patient-derived fibroblasts [18,29]. We assessed CME through fluorescent transferrin uptake measurement in the healthy control and the 2 DNM2-CNM fibroblast cell lines. Under basal conditions, CME was decreased in fibroblasts harbouring the R522H mutation (R522H-fibroblasts) and increased in fibroblasts harbouring the S619L mutation (S619L-fibroblasts) compared to control fibroblasts (Figure 7A) and western blot showed similar expression of transferrin receptor between control and mutant cells (Supp Figure 8). Among the AS-siRNA identified by our *in vitro* screening, we used si8 against the C version of the SNP1 (SNP1-si8-C, thereafter called siSNP1), si11 against the T version of the SNP2 (SNP2-si11-T, thereafter called siSNP2), and si10 against the p.S619L mutation (S619L-si10, thereafter called siS619) for the functional evaluation (Supp Figure 7). The decrease in transferrin uptake noticed in R522H-fibroblasts was unchanged by siSNP1 and siSNP2 when transfected at 30 nM for 48 hours (Figure 7B). At 100 nM, the values of transferrin uptake were increased by siSNP1 and siSNP2 close to the control values for siSNP1after 48 hours (Figure 7C). For the S619L-fibroblasts, the increase in transferrin was significantly reduced by siS619L and siSNP1 transfected at 30 nM and this is maintained at 100 nM (Figure 7B and C).

By measuring cell surface for transferrin uptake quantification, a defect was evidenced with a significantly smaller size for the R522H-fibroblasts and bigger size for the S619L-fibroblasts compared to the control cell line (Figure 7D). The impact of transfection of the 3 AS-siRNA of interest was then evaluated on the cell surface changes in patient-derived cells (Figures 7E and

7F). Among the tested AS-siRNA, siSNP2 improved the cell size of the R522H-fibroblasts when transfected at 100 nM. For the S619L-fibroblasts, siSNP1 improved the cell size from 30 nM and siS619L was able to restore cell size only when transfected at 100 nM. Overall, AS-siRNA directed against non-pathogenic SNPs were found to be as effective as AS-siRNA directly targeting the mutated nucleotide to restore CME and cell surface in patient-derived cells harbouring two distinct *DNM2* mutations.

Rescue of cell migration by AS-siRNA

DNM2 dysfunction through its overexpression is known to promote cell migration, invasion and metastasis in cancers [12]. Therefore, we looked for migration defects in the 2 fibroblast cell lines carrying the p.R522H and the p.S619L CNM mutations. We have tracked single cells during 24h and compared the motility behaviour in the 2 patient-derived cell lines and 2 healthy control cell lines. Both controls cells present similar motility behaviour (Figure 8A and Supp Figure 9A) but mutated fibroblasts presented cell motility defects including a reduced mean speed (Figure 8A), an increased duration of pause and a reduced speed when moving only for the S619L-fibroblasts (Supp Figure 9A).

To assess the benefit of allele-specific siRNA, we performed the same experiment 48h after cell transfection with either scramble siRNA or allele-specific siRNA (Supp Figure 7). At the concentration of 30 nM, all measured parameters are impaired in mutant fibroblasts transfected with scramble siRNA compared with the control cell line transfected with a scramble. At this concentration, siSNP1 improved all impaired motility parameters in the R522H-fibroblasts (*i.e.* mean speed, number and duration of pause and speed in motion). The siSNP2 fully rescued all the parameters at the control values (Figure 8B and Supp Figure 9B). For the S619L fibroblasts, siSNP1 and siS619L were effective to rescue or nearly rescuing the motility parameters to the control values (Figure 8B and Supp Figure 9B). A second set of experiments was performed at

100 nM final concentration to evaluate the possibility of a full restoration of motility parameters for siSNP1 in the R522H cells. As shown in Figure 8C and Supp Figure 9C, 100 nM of siSNP1 rescued all the motility parameters. Altogether these results highlight a decrease in cell motility associated with DNM2-CNM mutations which is restored using allele-specific siRNA.

Rescue of cell adhesion by AS-siRNA

The defects of both plasma membrane turnover due to endocytosis impairment and cell migration evidenced in the *DNM2*-mutated cell lines (Figures 7 and 8) may also suggest an impact of the *DNM2* mutations on cell adhesion. We next assessed the adhesion capacity of the 2 CNM fibroblast cell lines by quantifying the number of adherent cells per μm^2 1 hour after seeding on glass coverslips. A decrease of cell density around 60% was measured in the S619L-fibroblasts compared to control and no change occurred in the R522H-fibroblasts (Figure 8D). Consequently, we evaluated the impact of AS-siRNA transfected for 48 hours only in S619L-fibroblasts. At 30 nM, siS619L and siSNP1 were unable to revert the adhesion defect (Figure 8E) whereas a partial rescue was achieved at 100 nM as intermediate values between patient-derived cells and healthy control cells values were measured (Figure 8F). Overall, these results showed that adhesion defect may be present in CNM patient-derived cells and that selected AS-siRNA against one SNP or the mutation similarly improve this phenotype.

Discussion

Efficient silencing of morbid genes by RNA interference (RNAi) has been at the origin of several clinical trials. Efficacy and specificity of RNAi were also used to specifically target the mutated allele in dominant inherited diseases as for the most frequent *DNM2* mutation causing CNM which is due to a single nucleotide change[22]. One bottleneck which may limit the development of therapy by AS-RNAi for the *DNM2*-linked CNM, and beyond for the other diseases linked to *DNM2* mutations, is the number of reported *DNM2* mutations and then the number of required AS-siRNA required to cover the entire patient population. Here, we addressed this key point for preclinical development of AS-RNAi therapy for AD-CNM by developing versatile AS-siRNA against two non-pathogenic SNPs displaying a wide spectrum of application for the *DNM2*-linked diseases.

Allele-specific siRNA against SNP have been first developed in Huntington's disease [26–28,30,31] and Spinocerebellar ataxia [27,32] due to the nature of the mutation; i.e. a repeated sequence also carried by the normal allele in a shorter version which makes it difficult to develop siRNA targeting directly the disease-associated sequence. For these diseases, the development of siRNAs benefited from the presence of SNPs linked to the mutations. There is no disease-associated SNP in the *DNM2*-linked dominant centronuclear myopathy but the development of a similar strategy was made possible by the presence of two SNPs with a high frequency of heterozygosity (SNP1: 45% and SNP2: 30%). By this strategy, all the *DNM2* mutations can be silenced by choosing the siRNA against the version of the heterozygous SNP carried by the mutated mRNA. Consequently, we developed efficient AS-siRNA able to specifically silence each version of the 2 DNM2 SNPs. Relative to their frequency of heterozygosity in the population, siRNA against only these 4 targets allows covering ~60% of the AD-CNM patients. By adding the previously developed siRNA against the most frequent p.R645W mutation (27%

of patients) [17] and the siRNA also developed in this study devoted to silence the most frequent p.S619L mutation associated with the severe neonatal form of the disease (11% of patients) [17], ~75% of the AD-CNM population is covered.

One key step for the preclinical development of the AS-siRNA is the proof of principle for a therapeutic benefit in patient-derived cells using pertinent read-out related to the CNM pathomechanisms. Past studies have given contradictory results concerning the effect of CNM-associated *DNM2* mutations on clathrin-dependent endocytosis, some showing a decrease [18,29], others an absence of effect [33,34] or even an increase[35]. Despite these discrepancies, highlighting potential cell type- and/or mutation-specific impacts, we evaluated this canonical role attributed to DNM2. As previously [18], we show that clathrin-mediated endocytosis is impaired in patient fibroblasts and then may be used as a functional read-out for evaluating allele-specific siRNA. Interestingly, our results point towards distinct impacts relative to the DNM2 mutation as the R522H reduces endocytosis whereas the S619L leads to increased endocytosis. We may hypothesize that these opposite impacts may participate in the diversity of the clinical spectrum associated with DNM2 mutations. To identify additional readout, we took advantage of the growing number of studies showing the involvement of DNM2 dysfunction in the invasive behaviour of cancer cells [10,11,36–43] to evaluate the migration of cells carrying CNM mutations. Indeed, DNM2 dysfunction induced by both R522H and S619L mutations similarly impairs patient-derived cells' migratory properties. In contrast, only the S619L mutation associated with the severe neonatal CNM form also impedes cell adhesion. Like for clathrin-mediated endocytosis, the particular alteration of cell adhesion associated with the S619L mutation may start to highlight the cause of the clinical variability and especially the cause of the severe neonatal phenotype. Overall, our results represent a new argument in favour of impairment of the clathrin-mediated endocytosis by CNM-DNM2 mutations and highlight two new potential pathomechanisms through alteration of cell migration and adhesion. Further assessment will be

required in a muscle context for a better characterization of the pathomechanisms in the DNM2-CNM as such migration and adhesion impairments may participate in the reduced muscle regeneration recently demonstrated in a mouse model of the disease [44]. In addition, this work allowed us to identify a panel of readouts for the functional evaluation of the AS-siRNA.

Functional evaluation was performed for the new AS-siRNA developed against the S619L mutation and the two SNP. By this study, we showed that, except for adhesion, which is only partially restored, endocytosis, cell size, and cell migration are rescued by siS619 and siSNP1 in S619L-fibroblasts. In R522H-fibroblasts, endocytosis, size and migration have been similarly partially or fully restored by the AS-siRNA against the two SNPs. Beyond the efficacy obtained for each AS-siRNA, this study demonstrates that a similar benefit is reached using a siRNA targeting a mutation or a SNP. In addition, results obtained in the R522H-fibroblasts show that siRNA developed against SNP1 located in the coding region and SNP2 located in the 3'-UTR region are similarly efficient. However, regardless of the siRNA used, some defects are difficult to fully correct as illustrated by adhesion impairment in the S619L cells. Such a highly integrated cell process may require a longer time to be restored. Nevertheless, the functional evaluation showed that all the allele-specific siRNA developed against the S619L mutation and the two SNPs are largely efficient to rescue the defects identified in two patient-derived cell lines without inducing cell toxicity even at 100nM.

Interestingly, the field of application of versatile siRNAs against SNPs goes far beyond the *DNM2*-linked CNM as these siRNAs may also be used for the other dominant diseases due to *DNM2* mutations including dominant forms of the Charcot-Marie-Tooth disease (CMT) and hereditary spastic paraplegia (HSP). Due to the respective frequency of heterozygosity in humans, the development of the versatile siRNA may allow allele-specific silencing therapy in ~60% (according to frequency of heterozygosity reported in gnomAD) of the CMT and HSP patient population. The field of application of the versatile siRNAs is even wider since it also

386 includes 60% of patients affected by diseases in which a deleterious overexpression of DNM2
387 has been reported such as several cancers [12] and the X-linked recessive CNM [13]. The allele-
388 specific siRNA developed in this study against the SNP may be used in these pathological
389 conditions to reduce DNM2 expression in a controlled manner which avoids an excessive and
390 potential toxic reduction below 50% by sparing one allele.

391 In conclusion, this study enriches the molecular toolbox with several novel allele-specific
392 siRNA directed against the most frequent *DNM2* mutation responsible for the severe neonatal
393 dominant CNM and with versatile siRNA developed against two non-pathogenic SNPs able to
394 target all the *DNM2* mutations. These new molecular tools also enlarge the number of patients
395 eligible for the therapy by allele-specific DNM2 silencing by including diseases associated with
396 either *DNM2* mutations or deleterious overexpression. The current proof of concept in patient-
397 derived cells represents an important step for the preclinical development of this therapy for
398 AD-CNM patients.
399

Methods

Cell cultures and transfection

Healthy controls and CNM patient-derived fibroblast cell lines were obtained from the MyoLine platform for the immortalization of human cells (Institute of Myology, Paris, France) in accordance with European recommendations and French legislation. Cell lines were cultured at 37°C (5% CO_2) in Dulbecco's modified Eagle's medium (DMEM, Life Technologies, France) containing 10% fetal calf serum (FCS) supplemented with Penicillin (100 Units/ml) and Streptomycin (100 µg/ml). Patient and control fibroblasts were immortalized using a lentiviral vector containing the sequence encoding the catalytic subunit of human telomerase (hTERT) as previously described [45]. For transfection, cells were grown to 70% confluency and transfected with siRNAs using RNAimax transfection reagent (Life Technologies, France) according to the manufacturer's protocol. The concentration of siRNAs for each experiment was indicated in corresponding figure legends. Allele-specific siRNA and scramble siRNA were purchased from Eurogentec (Belgium) and the sequences are available on request. Cells were used for functional evaluation or harvested for RNA and protein extraction 48h after transfection.

Total RNA extraction and cDNA analysis

Total RNAs were isolated from cells using NucleoSpin RNA (Macherey-Nagel, France) according to the manufacturer's protocol. Cells were passed through a pipetting up-down several times for disruption in the lysis buffer. Total RNAs (500 ng) were submitted to reverse transcription using the Superscript III reverse transcriptase kit (Life Technologies, France) using oligo-dT primers in a final volume of 20 µl. Reverse transcription was performed at 50°C for 50 minutes, and a final step of 85°C for 5 minutes was added. To determine the allelic

version of each SNP present on the mutated allele, PCR encompassing SNPs and the mutation was performed and cloned using the pGEMT vector system (Promega) and about ten single clones were sequenced (Eurofins, France). The *DNM2* expression was quantified by semi-quantitative RT–PCR relative to the *HPRT* housekeeping gene expression. RT product (1 µl) was submitted to PCR performed at 96°C for 3 minutes followed by 27 cycles including denaturation at 96°C for 25 seconds, annealing at 58°C for 25 seconds and polymerization at 72°C for 40 seconds and a final step at 72°C for 5 minutes. The number of 27 PCR cycles has been selected to have the amplification in the exponential range for *DNM2* and *HPRT*. To quantify allele-specificity of the assessed siRNA, assays were developed for SNP1 and SNP2 using restriction enzymes allowing discrimination between the 2 alleles after digestion of the RT-PCR products. PCR was designed to amplify regions of the *DNM2* transcript encompassing the SNPs. RT product (1 µl) was submitted to SNP1 or SNP2 PCR performed at 96°C for 3 minutes followed by 40 cycles including denaturation at 96°C for 25 seconds, annealing at 58°C for 25 seconds and polymerization at 72°C for 40 seconds and a final step at 72°C for 5 minutes. The number of cycles has been selected to be at the end of the exponential phase of amplification. Ten µl out of the 20 µl PCR products were digested overnight at 37°C using 7 units of BglI (New England Biolabs, France) for SNP1, and 15 µl out of the 30 µl PCR products were digested overnight at 37°C using 7 units of Psp5II (New England Biolabs, France) for SNP2. Image acquisition of the PCR products after agarose gel electrophoresis was performed using a Geni2 gel imaging system (Ozyme, France), and the associated signal was quantified using ImageJ Software (NIH; http://rsbweb.nih.gov/ij). All the PCR primers used in this study were from Eurogentec (Belgium) and sequences are available on request.

Protein extraction and western blot

Cell pellets were homogenized in lysis buffer containing 50 mM of Tris-HCl pH 7.5, 150 mM NaCl, 1% IGEPAL, 0.5% Deoxycholate Sodium and protease inhibitor cocktail 1% (Sigma-Aldrich, France) and kept on rotator for 20 minutes at 4°C. After cell lysates scraping, samples are lysed by sonication 2 times for 10 seconds at 30% of a maximum power of VCX 130 Vibra-cell ultrasonic processors (Sonics, USA). After centrifugation (12,000 *g*, 4°C, 20 minutes), protein concentration in the supernatant was determined with the BCA Protein Assay Kit (Thermo Scientific Pierce, France). Five micrograms of proteins were mixed with a loading buffer (50 mM Tris-HCl, SDS 2%, glycerol 10%, β-mercaptoethanol 1% and bromophenol blue) and denatured at 90°C for 5 minutes. Protein samples were separated on SDS–PAGE 10% pre-stained gels and transferred onto PVDF membranes (0.45 µm pore size, Life Technologies, France) overnight at 100 mA at 4°C or nitrocellulose membranes (BioRad Turbo transfer System) by trans blot at 25V, 2.5 mA for 8 minutes. Membranes were blocked for 2 hours at room temperature in PBS containing non-fat dry milk 5% and Tween-20 0.1% and then exposed to rabbit polyclonal anti-Dynamin 2 antibody (ab3457 or ab65556, Abcam, France) or rabbit polyclonal anti-Transferrin receptor antibody (ab84036, Abcam, France) or rabbit polyclonal anti-GAPDH antibody (sc-25778 Santa Cruz, France) in PBS–Tween-20 0.1%, non-fat dry milk 1% overnight at 4°C. Membranes were rinsed in PBS–Tween-20 0.1% and incubated 2 hours with horseradish peroxidase-conjugated secondary antibody (anti-rabbit from Jackson ImmunoResearch, United Kingdom) in PBS–Tween-20 0.1%. Chemiluminescence was detected using ECL detection Kit (Merck-Millipore, Germany) in a BioRad Chemidoc MP imaging system and signal quantification was performed using ImageJ software.

Transferrin uptake assay and cell surface

Transfected cells were cultured in DMEM at 37°C for 45 minutes. Transferrin-AlexaFluor488 (Life Technologies, France) was added at 20 µg/ml at 37°C for 15 minutes. Cells were then

washed in DMEM pH 2 and PBS and fixed in paraformaldehyde 4% for 15 minutes. Images z-stacks were acquired using an Axio Observer Apotome.2 microscope (Zeiss, Germany) using a 20x Plan Apochromat Zeiss objective. Individual cells were outlined manually on the sum projection of the confocal stacks to measure cell surface (μm^2) and the transferrin uptake was calculated using the ImageJ software for each cell according to the formula: total corrected cell fluorescence (CTCF) = integrated density of the cell – (mean fluorescence of background x cell area).

Adhesion assay

Cells were harvested by trypsinization 48 hours after transfection or under basal conditions and 35000 cells were seeded on a 12-millimetre diameter glass coverslip in 24-well-plates (3 technical replicates for each transfection). After 1 hour incubation at 37°C in DMEM-10% FCS supplemented with Penicillin (100 Units/ml) and Streptomycin (100 µg/ml), the non-attached cells were removed by PBS washing and cells attached on coverslips were fixed in paraformaldehyde 4% for 15 minutes. Glass coverslips were mounted on slides with Vectashield medium (Vector Laboratories) containing DAPI to stain nuclei. Images were acquired using an Axio Observer Apotome.2 microscope (Zeiss, Germany) using a 2.5x Plan NeoFluar Zeiss objective and the number of attached cells per µm2 of coverslip were counted using ImageJ software through the counting of nuclei. Three independent experiments were done for each condition.

Cell tracking and analysis

Cells were seeded at low density on 24-wells plastic plates under basal conditions or 48 hours after transfection. Bright-field images were acquired at 10X magnification every 20 or 30 minutes (for transfected cells and basal condition, respectively) for 65 hours using an inverted

video-microscope equipped with heat and CO_2 controlled chamber (Nikon Ti2, Oko-Lab) driven by NIS (Nikon). After reconstruction of a 24-hour movie, 50 to 70 cells per condition were randomly chosen and manually tracked by following the position of the nuclei using ImageJ software and MTrackJ plugin to determine mean and max speed [46]. Others motility parameters (mean speed in motion, number and duration of pause) were obtained using Skypad Microsoft Excel add-in that automatically analyzes particles in 2D trajectories[47]. A threshold of 10 µm was set out to consider the cell in movement between two-time frames and a speed threshold of 0.1 µm/minute was set out to consider a relevant displacement.

Data analysis and statistics

Graphics and statistical analyses were performed with GraphPad Prism software versions 6 or 9 (GraphPad Software, LaJolla, California, USA). Values were expressed as means ± SEM. The number of samples (n), represents the number of independent biological replicates, as indicated in the figure legends. Number of values analyzed, mean and SEM for all the graph presented in the figures are listed as supplementary table 1.

We used non-parametric statistical tests to analyze our data when the normality could not be assumed (Shapiro-Wilk test) or tested (n too small). In this case, statistical comparisons between groups were performed using unpaired two-tailed Mann–Whitney *U*-test for the siRNAs screening or using a Kruskal-Wallis test followed when significant by Dunn's for transferrin uptake, cell size and migration assays. Adhesion assay was analyzed using Anova followed by Bonferroni post-test or Welch's ANOVA to correct the inequality of variance followed Dunnett's as post-test. P values indicated for Post hoc tests are adjusted p value. $P < 0.05$ were considered as statistically significant.

Acknowledgements

We acknowledge the Platform for Immortalization of Human Cells at the Institut de Myologie, (Paris, France) for the generation and distribution of the human cell lines. This work was supported by the Institut National de la Santé et de la Recherche Médicale (Inserm), Inserm Transfert (CoPoC grant), the Association Institut de Myologie (AIM), Sorbonne Université, and the Agence Nationale de la Recherche ANR (Dynather, ANR-18-CE17-0006-02 to MB).

Author contributions

DT and MB conceived and designed the experiments. SD, LM, BP, KM, DT, and MB performed the experiments. SD, LM, DT, and MB analyzed the data. DT and MB wrote the manuscript.

Conflict of interest statement: The authors have declared that no conflict of interest exists.

Keywords: allele-specific silencing therapy; dominant centronuclear myopathy; Dynamin 2; RNA interference, endocytosis, migration, adhesion.

Data Availability Statement:

References

1. Romero, N.B., and Bitoun, M. (2011). Centronuclear myopathies. Semin Pediatr Neurol *18*, 250–6.

2. Hanisch, F., Muller, T., Dietz, A., Bitoun, M., Kress, W., Weis, J., Stoltenburg, G., and Zierz, S. (2011). Phenotype variability and histopathological findings in centronuclear myopathy due to DNM2 mutations. J Neurol *258*, 1085–1090.

3. Bitoun, M., Bevilacqua, J.A., Prudhon, B., Maugenre, S., Taratuto, A.L., Monges, S., Lubieniecki, F., Cances, C., Uro-Coste, E., Mayer, M., et al. (2007). Dynamin 2 mutations cause sporadic centronuclear myopathy with neonatal onset. Ann Neurol *62*, 666–70.

4. Bitoun, M., Maugenre, S., Jeannet, P.Y., Lacène, E., Ferrer, X., Laforêt, P., Martin, J.J., Laporte, J., Lochmuller, H., Beggs, A.H., et al. (2005). Mutations in dynamin 2 cause dominant Centronuclear Myopathy. Nature Genet *37*, 1207–1209.

5. Zuchner, S., Noureddine, M., Kennerson, M., Verhoeven, K., Claeys, K., De Jonghe, P., Merory, J., Oliveira, S.A., Speer, M.C., Stenger, J.E., et al. (2005). Mutations in the pleckstrin homology domain of dynamin 2 cause dominant intermediate Charcot-Marie-Tooth disease. Nat Genet *37*, 289–94.

6. Sambuughin, N., Goldfarb, L.G., Sivtseva, T.M., Davydova, T.K., Vladimirtsev, V.A., Osakovskiy, V.L., Danilova, A.P., Nikitina, R.S., Ylakhova, A.N., Diachkovskaya, M.P., et al. (2015). Adult-onset autosomal dominant spastic paraplegia linked to a GTPase-effector domain mutation of dynamin 2. BMC Neurol *15*, 223.

7. Raja, S., Shah, S., Tariq, A., Bibi, N., Sughra, K., Yousuf, A., Khawaja, A., Nawaz, M., Mehmood, A., Khan, M., et al. (2019). Caveolin-1 and dynamin-2 overexpression is associated with the progression of bladder cancer. Oncol Lett.

8. Ren, N., Tian, Z., Sun, H., and Lu, X. (2020). Dynamin 2 Is Correlated with Recurrence and Poor Prognosis of Papillary Thyroid Cancer. Med. Sci. Monit. *26*, e924590.

9. Chernikova, S.B., Nguyen, R.B., Truong, J.T., Mello, S.S., Stafford, J.H., Hay, M.P., Olson, A., Solow-Cordero, D.E., Wood, D.J., Henry, S., et al. (2018). Dynamin impacts homology-directed repair and breast cancer response to chemotherapy. J Clin Invest *128*, 5307–5321.

10. Eppinga, R.D., Krueger, E.W., Weller, S.G., Zhang, L., Cao, H., and McNiven, M.A. (2012). Increased expression of the large GTPase dynamin 2 potentiates metastatic migration and invasion of pancreatic ductal carcinoma. Oncogene *31*, 1228–41.

11. Xu, B., Teng, L.H., Silva, S.D., Bijian, K., Al Bashir, S., Jie, S., Dolph, M., Alaoui-Jamali, M.A., and Bismar, T.A. (2014). The significance of dynamin 2 expression for prostate cancer progression, prognostication, and therapeutic targeting. Cancer Med *3*, 14–24.

12. Trochet, D., and Bitoun, M. (2021). A review of Dynamin 2 involvement in cancers highlights a promising therapeutic target. J Exp Clin Cancer Res *40*, 238.

13. Cowling, B.S., Chevremont, T., Prokic, I., Kretz, C., Ferry, A., Coirault, C., Koutsopoulos, O., Laugel, V., Romero, N.B., and Laporte, J. (2014). Reducing dynamin 2 expression rescues X-linked centronuclear myopathy. J Clin Invest *124*, 1350–63.

14. Heymann, J.A., and Hinshaw, J.E. (2009). Dynamins at a glance. J Cell Sci *122*, 3427–31.

15. Ferguson, S.M., and De Camilli, P. (2012). Dynamin, a membrane-remodelling GTPase. Nat Rev Mol Cell Biol *13*, 75–88.

16. Durieux, A.C., Prudhon, B., Guicheney, P., and Bitoun, M. (2010). Dynamin 2 and Human diseases. J Mol Med *88*, 339–350.

17. Bohm, J., Biancalana, V., Dechene, E.T., Bitoun, M., Pierson, C.R., Schaefer, E., Karasoy, H., Dempsey, M.A., Klein, F., Dondaine, N., et al. (2012). Mutation spectrum in the

large GTPase dynamin 2, and genotype-phenotype correlation in autosomal dominant centronuclear myopathy. Hum Mutat *33*, 949–59.

18. Bitoun, M., Durieux, A.C., Prudhon, B., Bevilacqua, J.A., Herledan, A., Sakanyan, V., Urtizberea, A., Cartier, L., Romero, N.B., and Guicheney, P. (2009). Dynamin 2 mutations associated with human diseases impair clathrin-mediated receptor endocytosis. Hum Mutat *30*, 1419–27.

19. Kenniston, J.A., and Lemmon, M.A. (2010). Dynamin GTPase regulation is altered by PH domain mutations found in centronuclear myopathy patients. EMBO J *29*, 3054–67.

20. Wang, L., Barylko, B., Byers, C., Ross, J.A., Jameson, D.M., and Albanesi, J.P. (2010). Dynamin 2 mutants linked to centronuclear myopathies form abnormally stable polymers. J Biol Chem *285*, 22753–7.

21. Ferguson, S., Raimondi, A., Paradise, S., Shen, H., Mesaki, K., Ferguson, A., Destaing, O., Ko, G., Takasaki, J., Cremona, O., et al. (2009). Coordinated actions of actin and BAR proteins upstream of dynamin at endocytic clathrin-coated pits. Dev Cell *17*, 811–22.

22. Trochet, D., Prudhon, B., Beuvin, M., Peccate, C., Lorain, S., Julien, L., Benkhelifa-Ziyyat, S., Rabai, A., Mamchaoui, K., Ferry, A., et al. (2018). Allele-specific silencing therapy for Dynamin 2-related dominant centronuclear myopathy. EMBO Mol Med *10*, 239–253.

23. Trochet, D., Prudhon, B., Vassilopoulos, S., and Bitoun, M. (2015). Therapy for Dominant Inherited Diseases by Allele-Specific RNA Interference: Successes and Pitfalls. Curr Gene Ther *15*, 503–10.

24. Leachman, S.A., Hickerson, R.P., Schwartz, M.E., Bullough, E.E., Hutcherson, S.L., Boucher, K.M., Hansen, C.D., Eliason, M.J., Srivatsa, G.S., Kornbrust, D.J., et al. (2010). First-in-human mutation-targeted siRNA phase Ib trial of an inherited skin disorder. Mol Ther *18*, 442–6.

615 25. Golan, T., Khvalevsky, E.Z., Hubert, A., Gabai, R.M., Hen, N., Segal, A., Domb, A.,
616 Harari, G., David, E.B., Raskin, S., et al. (2015). RNAi therapy targeting KRAS in combination
617 with chemotherapy for locally advanced pancreatic cancer patients. Oncotarget *6*, 24560–70.
618 26. Lombardi, M.S., Jaspers, L., Spronkmans, C., Gellera, C., Taroni, F., Di Maria, E.,
619 Donato, S.D., and Kaemmerer, W.F. (2009). A majority of Huntington's disease patients may
620 be treatable by individualized allele-specific RNA interference. Exp Neurol *217*, 312–9.
621 27. Fiszer, A., Olejniczak, M., Switonski, P.M., Wroblewska, J.P., Wisniewska-Kruk, J.,
622 Mykowska, A., and Krzyzosiak, W.J. (2012). An evaluation of oligonucleotide-based
623 therapeutic strategies for polyQ diseases. BMC Mol Biol *13*, 6.
624 28. Takahashi, M., Watanabe, S., Murata, M., Furuya, H., Kanazawa, I., Wada, K., and
625 Hohjoh, H. (2010). Tailor-made RNAi knockdown against triplet repeat disease-causing alleles.
626 Proc Natl Acad Sci U S A *107*, 21731–6.
627 29. Ali, T., Bednarska, J., Vassilopoulos, S., Tran, M., Diakonov, I.A., Ziyadeh-Isleem, A.,
628 Guicheney, P., Gorelik, J., Korchev, Y.E., Reilly, M.M., et al. (2019). Correlative SICM-FCM
629 reveals changes in morphology and kinetics of endocytic pits induced by disease-associated
630 mutations in dynamin. FASEB J *33*, 8504–8518.
631 30. van Bilsen, P.H., Jaspers, L., Lombardi, M.S., Odekerken, J.C., Burright, E.N., and
632 Kaemmerer, W.F. (2008). Identification and allele-specific silencing of the mutant huntingtin
633 allele in Huntington's disease patient-derived fibroblasts. Hum Gene Ther *19*, 710–9.
634 31. Drouet, V., Ruiz, M., Zala, D., Feyeux, M., Auregan, G., Cambon, K., Troquier, L.,
635 Carpentier, J., Aubert, S., Merienne, N., et al. (2014). Allele-specific silencing of mutant
636 huntingtin in rodent brain and human stem cells. PLoS One *9*, e99341.
637 32. Scholefield, J., Watson, L., Smith, D., Greenberg, J., and Wood, M.J. (2014). Allele-
638 specific silencing of mutant Ataxin-7 in SCA7 patient-derived fibroblasts. Eur J Hum Genet.

33. Liu, Y.W., Lukiyanchuk, V., and Schmid, S.L. (2011). Common membrane trafficking defects of disease-associated dynamin 2 mutations. Traffic *12*, 1620–33.

34. Sidiropoulos, P.N., Miehe, M., Bock, T., Tinelli, E., Oertli, C.I., Kuner, R., Meijer, D., Wollscheid, B., Niemann, A., and Suter, U. (2012). Dynamin 2 mutations in Charcot-Marie-Tooth neuropathy highlight the importance of clathrin-mediated endocytosis in myelination. Brain *135*, 1395–411.

35. Rabai, A., Reisser, L., Reina-San-Martin, B., Mamchaoui, K., Cowling, B.S., Nicot, A.-S., and Laporte, J. (2019). Allele-Specific CRISPR/Cas9 Correction of a Heterozygous DNM2 Mutation Rescues Centronuclear Myopathy Cell Phenotypes. Mol Ther Nucleic Acids *16*, 246–256.

36. Burton, K.M., Cao, H., Chen, J., Qiang, L., Krueger, E.W., Johnson, K.M., Bamlet, W.R., Zhang, L., McNiven, M.A., and Razidlo, G.L. (2020). Dynamin 2 interacts with α-actinin 4 to drive tumor cell invasion. MBoC *31*, 439–451.

37. Yamada, H., Takeda, T., Michiue, H., Abe, T., and Takei, K. (2016). Actin bundling by dynamin 2 and cortactin is implicated in cell migration by stabilizing filopodia in human non-small cell lung carcinoma cells. International Journal of Oncology *49*, 877–886.

38. Zhang, Y., Nolan, M., Yamada, H., Watanabe, M., Nasu, Y., Takei, K., and Takeda, T. (2016). Dynamin2 GTPase contributes to invadopodia formation in invasive bladder cancer cells. Biochemical and Biophysical Research Communications *480*, 409–414.

39. Razidlo, G.L., Wang, Y., Chen, J., Krueger, E.W., Billadeau, D.D., and McNiven, M.A. (2013). Dynamin 2 potentiates invasive migration of pancreatic tumor cells through stabilization of the Rac1 GEF Vav1. Dev Cell *24*, 573–85.

40. Wong, B.S., Shea, D.J., Mistriotis, P., Tuntithavornwat, S., Law, R.A., Bieber, J.M., Zheng, L., and Konstantopoulos, K. (2019). A Direct Podocalyxin–Dynamin-2 Interaction

663 Regulates Cytoskeletal Dynamics to Promote Migration and Metastasis in Pancreatic Cancer
664 Cells. Cancer Res *79*, 2878–2891.
665 41. Yamada, H., Abe, T., Li, S.-A., Tago, S., Huang, P., Watanabe, M., Ikeda, S., Ogo, N.,
666 Asai, A., and Takei, K. (2014). N′-[4-(dipropylamino)benzylidene]-2-hydroxybenzohydrazide
667 is a dynamin GTPase inhibitor that suppresses cancer cell migration and invasion by inhibiting
668 actin polymerization. Biochemical and Biophysical Research Communications *443*, 511–517.
669 42. Baldassarre, M., Pompeo, A., Beznoussenko, G., Castaldi, C., Cortellino, S., McNiven,
670 M.A., Luini, A., and Buccione, R. (2003). Dynamin participates in focal extracellular matrix
671 degradation by invasive cells. Mol Biol Cell *14*, 1074–84.
672 43. Rosse, C., Lodillinsky, C., Fuhrmann, L., Nourieh, M., Monteiro, P., Irondelle, M.,
673 Lagoutte, E., Vacher, S., Waharte, F., Paul-Gilloteaux, P., et al. (2014). Control of MT1-MMP
674 transport by atypical PKC during breast-cancer progression. Proceedings of the National
675 Academy of Sciences *111*, E1872–E1879.
676 44. F Almeida, C., Bitoun, M., and Vainzof, M. (2021). Satellite cells deficiency and
677 defective regeneration in dynamin 2-related centronuclear myopathy. FASEB J *35*, e21346.
678 45. Auré, K., Mamchaoui, K., Frachon, P., Butler-Browne, G.S., Lombès, A., and Mouly,
679 V. (2007). Impact on oxidative phosphorylation of immortalization with the telomerase gene.
680 Neuromuscul Disord *17*, 368–375.
681 46. Meijering, E., Dzyubachyk, O., and Smal, I. (2012). Methods for cell and particle
682 tracking. Methods Enzymol *504*, 183–200.
683 47. Cadot, B., Gache, V., and Gomes, E.R. (2014). Fast, multi-dimensional and
684 simultaneous kymograph-like particle dynamics (SkyPad) analysis. PLoS One *9*, e89073.
685
686

List of Figure Captions

Figure 1. Identification of targetable SNPs and heterozygous cells. A. Schematic representation of the *DNM2* mRNA showing the location of 2 CNM-mutations and 2 single nucleotide polymorphisms (SNP). For each SNP, the frequencies of the 2 alleles are indicated as well as the frequency of heterozygosity in the population. HTZ: heterozygous. **B**. Sequencing of the SNPs in healthy control and 2 patient-derived cell lines. **C**. Results of the genotyping of SNP1 and SNP2 on the wild-type (WT) and mutated *DNM2* mRNAs in the 2 patient-derived cell lines.

Figure 2: Identification of allele-specific siRNA against the C version of SNP1. A. Expression of the *DNM2* mRNA 48 hours after siRNA transfection at 30 nM. Agarose gel electrophoresis of *DNM2* and *HPRT* RT-PCR products and quantification of *DNM2* expression normalized to *HPRT* ($n \geq 4$ per condition). **B**. BglI digestion profile on the *DNM2* PCR product including the SNP1 sequence and quantification of the C/T ratio ($n \geq 4$ per condition) after transfection with siRNA at 30 nM. **C**. Expression of the *DNM2* mRNA 48 hours after siRNA transfection at 100 nM. Agarose gel electrophoresis of *DNM2* and *HPRT* RT-PCR products and quantification of *DNM2* expression normalized to *HPRT* ($n \geq 4$ per condition). **D**. BglI digestion profile on the *DNM2* PCR product including the SNP1 sequence and quantification of the C/T ratio ($n \geq 4$ per condition) after transfection with siRNA at 100 nM. **E.** DNM2 western blot and quantification of the signal by densitometry after siRNA transfection at 100 nM concentration. GAPDH was used as a loading control ($n \geq 4$). Data information: In scatter plots, the bars are mean values and error bars indicate SEM. ****$P < 0.0001$, ***$P < 0.001$, **$P < 0.01$ and *$P < 0.5$ using a two-tailed Mann–Whitney *U*-test relative to the scramble siRNA (Sc).

Figure 3: Identification of allele-specific siRNA against the T version of SNP1. **A.** Expression of the *DNM2* mRNA 48 hours after siRNA transfection at 30 nM. Agarose gel electrophoresis of *DNM2* and *HPRT* RT-PCR products and quantification of *DNM2* expression normalized to *HPRT* (n ≥4 per condition). **B**. BglI digestion profile on the *DNM2* PCR product including the SNP1 sequence and quantification of the T/C ratio (n ≥4 per condition) after transfection with siRNA at 30 nM. **C**. Expression of the *DNM2* mRNA 48 hours after siRNA transfection at 100 nM. Agarose gel electrophoresis of *DNM2* and *HPRT* RT-PCR products and quantification of *DNM2* expression normalized to *HPRT* (n ≥4 per condition). **D**. BglI digestion profile on the *DNM2* PCR product including the SNP1 sequence and quantification of the T/C ratio (n ≥4 per condition) after transfection with siRNA at 100 nM. **E.** DNM2 western blot and quantification of the signal by densitometry after siRNA transfection at 100 nM concentration. GAPDH was used as a loading control (n ≥4). Data information: In scatter plots, the bars are mean values and error bars indicate SEM. *P < 0.5 using a two-tailed Mann–Whitney *U*-test relative to the scramble siRNA (Sc)

Figure 4: Identification of allele-specific siRNA against the T version of SNP2. A. Expression of the *DNM2* mRNA 48 hours after siRNA transfection at 30 nM. Agarose gel electrophoresis of *DNM2* and *HPRT* RT-PCR products and quantification of *DNM2* expression normalized to *HPRT* (n ≥4 per condition). **B**. Psp5II digestion profile on the *DNM2* PCR product including the SNP2 sequence and quantification of the T/A ratio (n ≥4 per condition) after transfection with siRNA at 30 nM. **C**. Expression of the *DNM2* mRNA 48 hours after siRNA transfection at 100 nM. Agarose gel electrophoresis of *DNM2* and *HPRT* RT-PCR products and quantification of *DNM2* expression normalized to *HPRT* (n ≥4 per condition). **D**. Psp5II digestion profile on the *DNM2* PCR product including the SNP2 sequence and quantification of the T/A ratio (n ≥4 per condition) after transfection with siRNA at 100 nM.

E. DNM2 western blot and quantification of the signal by densitometry after siRNA transfection at 100 nM concentration. GAPDH was used as a loading control (n ≥4). Data information: In scatter plots, the bars are mean values and error bars indicate SEM. ****P < 0.0001, ***P < 0.001, **P < 0.01 and *P < 0.5 using a two-tailed Mann–Whitney *U*-test relative to the scramble siRNA (Sc).

Figure 5: Identification of allele-specific siRNA against the A version of SNP2. **A.** Expression of the *DNM2* mRNA 48 hours after siRNA transfection at 30 nM. Agarose gel electrophoresis of *DNM2* and *HPRT* RT-PCR products and quantification of *DNM2* expression normalized to *HPRT* (n ≥4 per condition). **B**. Psp5II digestion profile on the *DNM2* PCR product including the SNP2 sequence and quantification of the A/T ratio (n ≥4 per condition) after transfection with siRNA at 30 nM. **C**. Expression of the *DNM2* mRNA 48 hours after siRNA transfection at 100 nM. Agarose gel electrophoresis of *DNM2* and *HPRT* RT-PCR products and quantification of *DNM2* expression normalized to *HPRT* (n ≥4 per condition). **D**. Psp5II digestion profile on the *DNM2* PCR product including the SNP2 sequence and quantification of the A/T ratio (n ≥4 per condition) after transfection with siRNA at 100 nM. **E.** DNM2 western blot and quantification of the signal by densitometry after siRNA transfection at 100 nM concentration. GAPDH was used as a loading control (n ≥4). Data information: In scatter plots, the bars are mean values and error bars indicate SEM. **P < 0.01 and *P < 0.5 using a two-tailed Mann–Whitney *U*-test relative to the scramble siRNA (Sc).

Figure 6: Identification of allele-specific siRNA against the S619L DNM2 mutation. A. Expression of the *DNM2* mRNA 48 hours after siRNA transfection at 30 nM. Agarose gel electrophoresis of *DNM2* and *HPRT* RT-PCR products and quantification of *DNM2* expression normalized to *HPRT* (n ≥4 per condition). **B**. BglI digestion profile on the DNM2 PCR product

761 including the SNP1 sequence and quantification of the mutant/WT ratio (n ≥4 per condition)
762 after transfection with siRNA at 30 nM. The mutant allele harbors the C version of SNP1. **C**.
763 Expression of the *DNM2* mRNA 48 hours after siRNA transfection at 100 nM. Agarose gel
764 electrophoresis of *DNM2* and *HPRT* RT-PCR products and quantification of *DNM2* expression
765 normalized to *HPRT* (n ≥4 per condition). **D**. BglI digestion profile on the *DNM2* PCR product
766 including the SNP1 sequence and quantification of the mutant/WT ratio (n ≥4 per condition)
767 after transfection with siRNA at 100 nM. **E.** DNM2 western blot and quantification of the signal
768 by densitometry after siRNA transfection at 100 nM concentration. GAPDH was used as a
769 loading control (n ≥4). Data information: In scatter plots, the bars are mean values and error
770 bars indicate SEM. ***P < 0.001 and *P < 0.1 using a two-tailed Mann–Whitney *U*-test relative
771 to the scramble siRNA (Sc)
772
773 **Figure 7: Impact of AS-siRNA on transferrin uptake and cell surface of patient-derived**
774 **fibroblasts. A**. Transferrin uptake under basal conditions (n= 500-700 cells from 3 independent
775 experiments). CTCF: Corrected total cell fluorescence. **B**. Transferrin uptake after 48 hours
776 transfection with 30 nM scramble siRNA (sc) or allele-specific siRNA against the S619L
777 mutation or the 2 SNPs (n= 200-300 cells from 2 independent experiments). **C**. Transferrin
778 uptake after 48 hours transfection with 100 nM scramble siRNA (sc) or allele-specific siRNA
779 against the S619L mutation or the 2 SNPs (n= 200-300 cells from 2 independent experiments).
780 **D**. Cell surface (μm^2) under basal conditions (n= 500-700 cells from 3 independent
781 experiments). **E**. Cell surface after 48 hours transfection with 30 nM scramble siRNA (sc) or
782 allele-specific siRNA against the S619L mutation or the 2 SNPs (n= 200-300 cells from 2
783 independent experiments). **F**. Cell surface after 48 hours transfection with 100 nM scramble
784 siRNA (sc) or allele-specific siRNA against the S619L mutation or the 2 SNPs (n= 200-300
785 cells from 2 independent experiments). Data information: bars represent mean values and error

bars indicate SEM. Statistical analysis are performed using Kruskal-Wallis for A to F (**** p<0.0001 in all histograms), followed by Dunn's test relative to control cells in A and D (**** P<0.0001, *** P<0.001 adjusted p-value), control cells transfected with scramble siRNA in B, C, E and F (**** P<0.0001 adjusted p-values), or the patient cell lines transfected with scramble siRNA in B, C, E and F († P<0.05, †† P<0.01, and †††† P<0.0001 adjusted p-values).

Figure 8: Migration and adhesion assays in patient-derived cells. A. Mean speed of CNM- and control-fibroblasts (µm/minute) under basal conditions (n=50 cells tracked). **B**. Mean speed of cells after 48 hours transfection with 30 nM scramble siRNA (sc) or allele-specific siRNA against the S619L mutation or the 2 SNPs (n= 50-70 cells tracked). **C**. Mean speed of cells after 48 hours transfection with 100 nM scramble siRNA (sc) or allele-specific siRNA against the SNP1 (n= 50-70 cells tracked). **D**. Adhesion under basal conditions (n=8 independent assays). **E**. Adhesion assay after 48 hours transfection with 30 nM scramble siRNA (sc) or allele-specific siRNA against the S619L mutation or the SNP1 (n=5 or 6 independent transfections). **F**. Adhesion assay after 48 hours transfection with 100 nM scramble siRNA (sc) or allele-specific siRNA against the S619L mutation or SNP1 (n=6 independent transfections). Data information: bars represent mean values and error bars indicate SEM. Statistical analysis are performed using Kruskal-Wallis for migration assay A to C (**** p<0.0001 in all histograms), followed by Dunn's test relative to control cells 1 (*** P<0.001) or control cells 2 (φφ P<0.01) in A, or to control cells transfected with scramble siRNA in B and C (**** P<0.0001), or to patient cell lines transfected with scramble siRNA in B and C (†††† P<0.0001). Anova tests were performed for adhesion assay in A (** P<0.01), B and C (****P<0.0001) followed by post-tests relative to control cells in A (**P<0.01), to control cells transfected with scramble siRNA (**** P<0.0001, *** P<0.001 ** P<0.01) and to patient cell lines transfected with scramble siRNA (†† p<0.01, †† p<0.05) in B and C

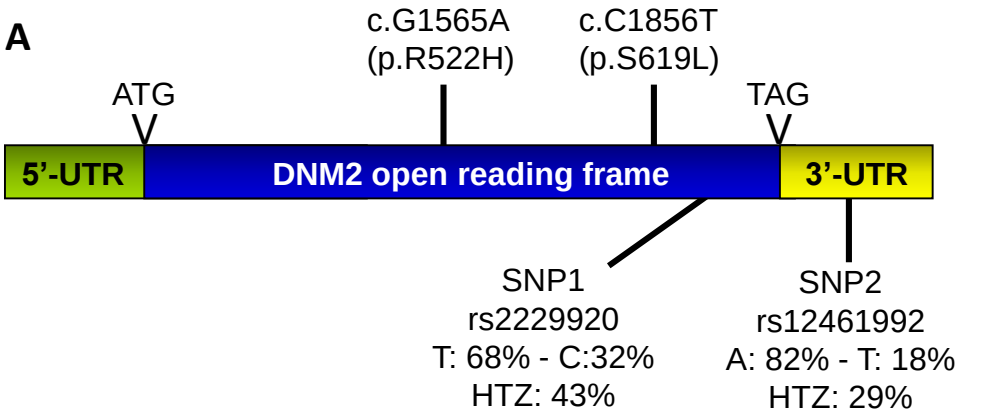
A
c.G1565A
(p.R522H)
c.C1856T
(p.S619L)
ATG
TAG
5'-UTR
DNM2 open reading frame
3'-UTR
SNP1
rs2229920
T: 68% - C:32%
HTZ: 43%
SNP2
rs12461992
A: 82% - T: 18%
HTZ: 29%

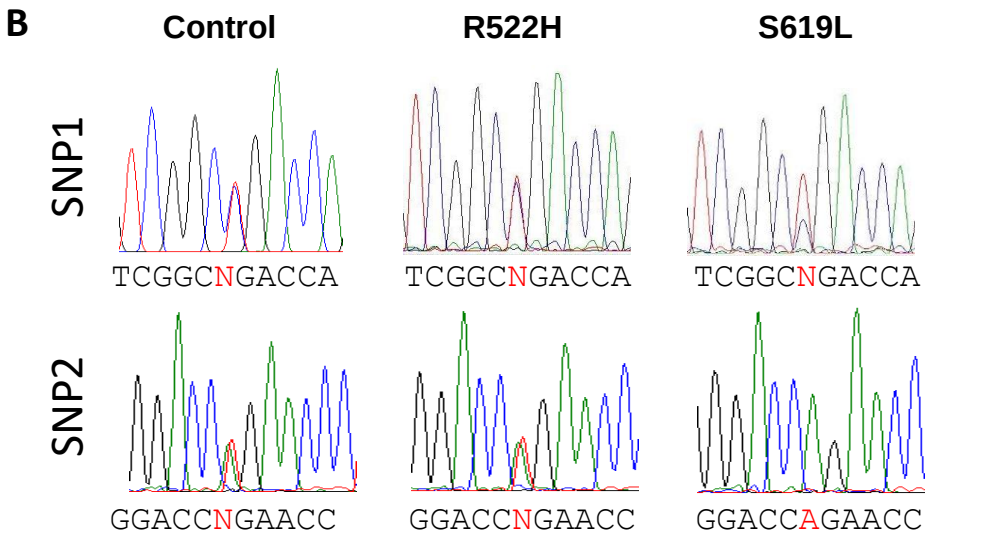
B
Control
R522H
S619L
SNP1
TCGGCNGACCA
TCGGCNGACCA
TCGGCNGACCA
SNP2
GGACCNGAACC
GGACCNGAACC
GGACCAGAACC

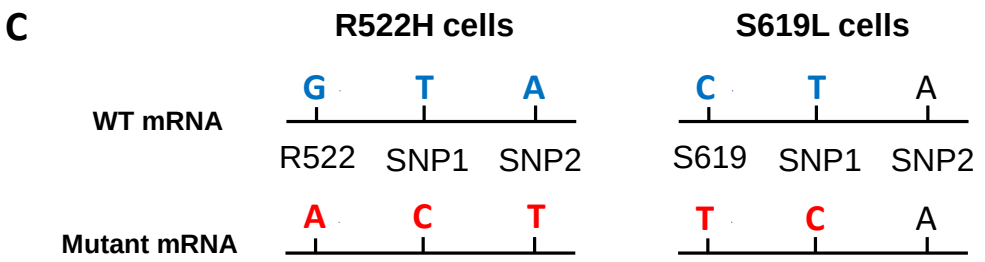
C
R522H cells
S619L cells
WT mRNA
G
T
A
R522
SNP1
SNP2
C
T
A
S619
SNP1
SNP2
Mutant mRNA
A
C
T
T
C
A

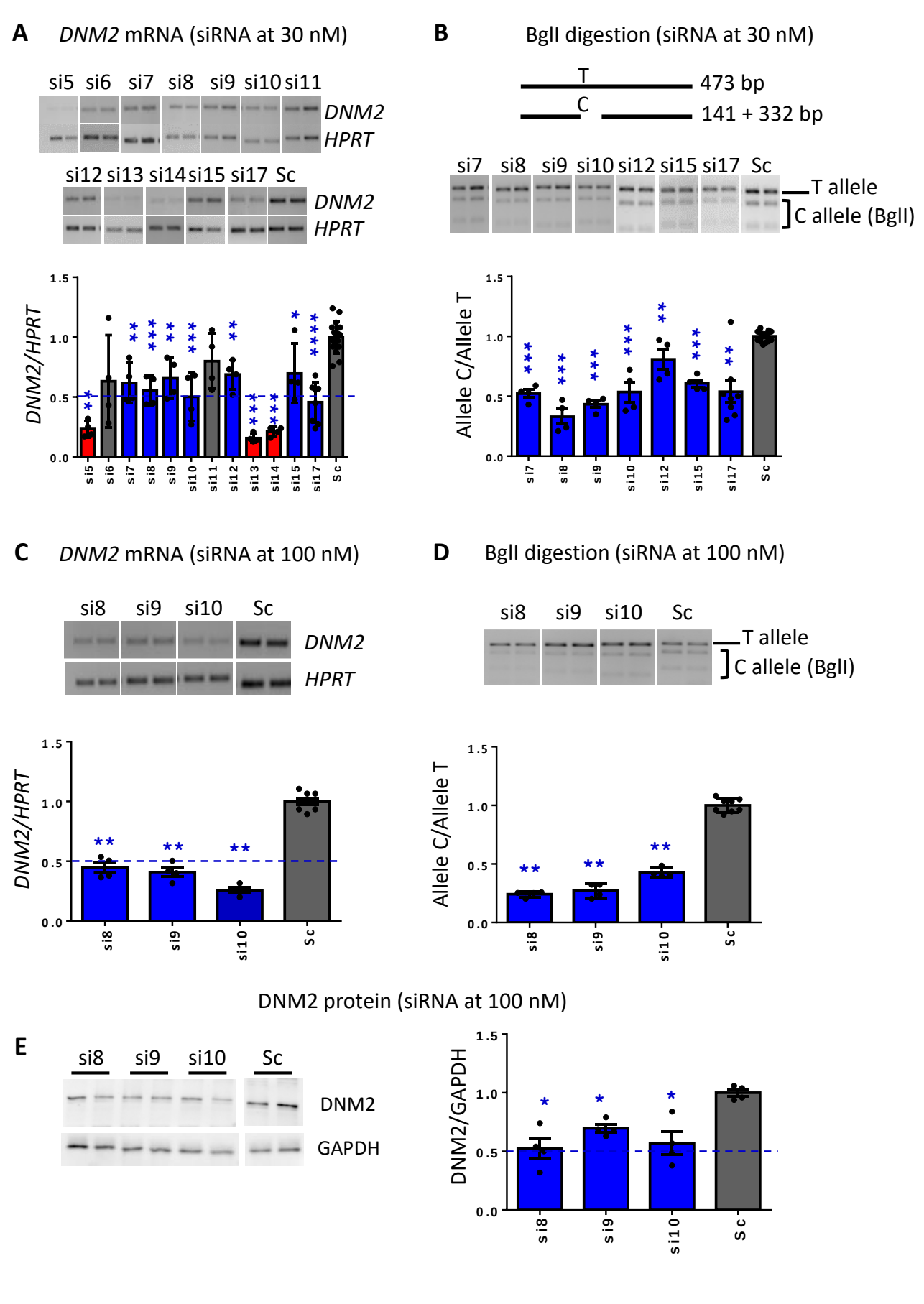
A
DNM2 mRNA (siRNA at 30 nM)
si5 si6 si7 si8 si9 si10 si11
DNM2
HPRT
si12 si13 si14 si15 si17 Sc
DNM2
HPRT
DNM2/HPRT
B
BglI digestion (siRNA at 30 nM)
T
C
473 bp
141 + 332 bp
si7 si8 si9 si10 si12 si15 si17 Sc
T allele
C allele (BglI)
Allele C/Allele T
C
DNM2 mRNA (siRNA at 100 nM)
si8 si9 si10 Sc
DNM2
HPRT
DNM2/HPRT
D
BglI digestion (siRNA at 100 nM)
si8 si9 si10 Sc
T allele
C allele (BglI)
Allele C/Allele T
DNM2 protein (siRNA at 100 nM)
E
si8 si9 si10 Sc
DNM2
GAPDH
DNM2/GAPDH

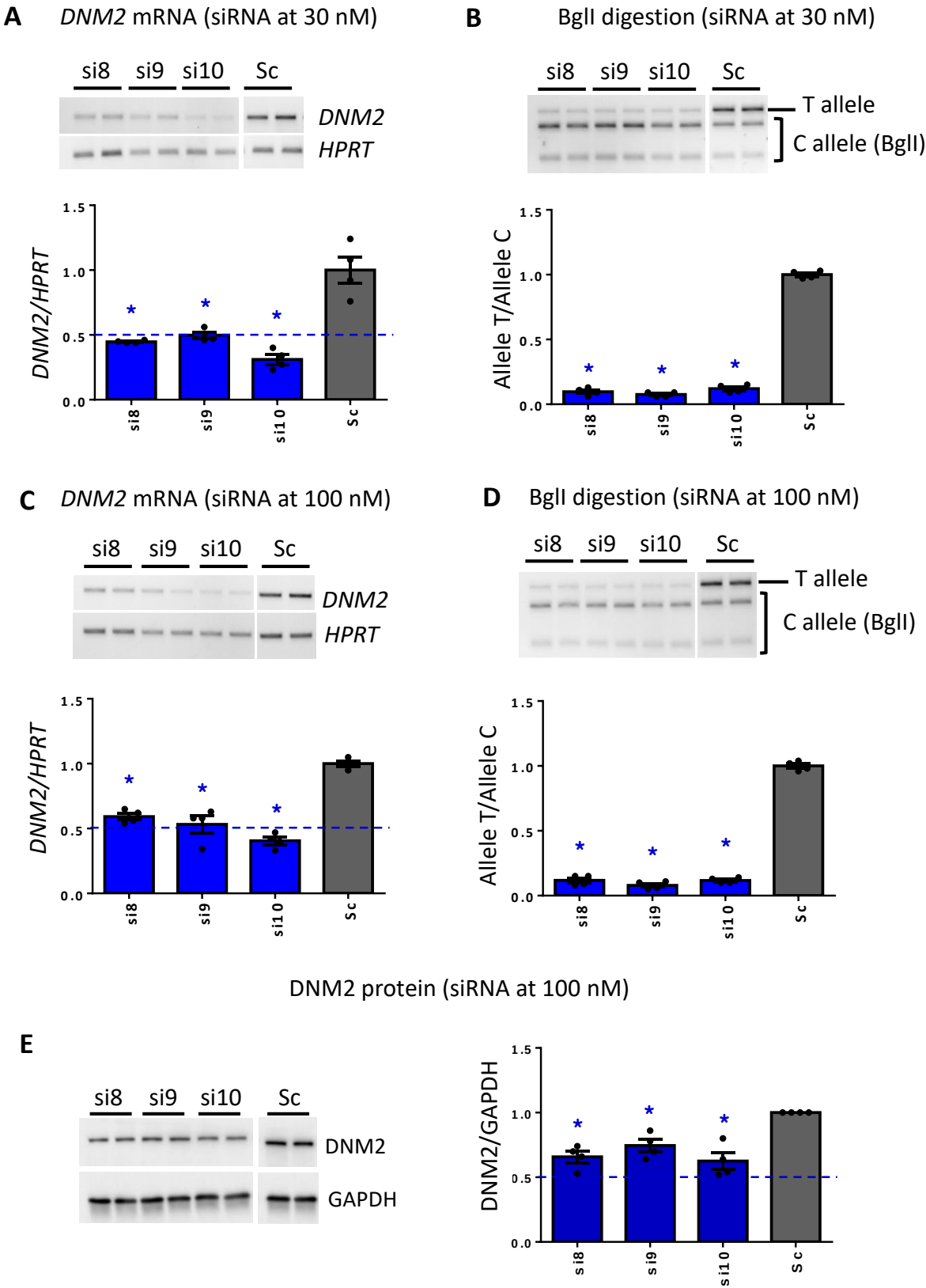
A
DNM2 mRNA (siRNA at 30 nM)
si8
si9
si10
Sc
DNM2
HPRT
DNM2/HPRT
B
BglI digestion (siRNA at 30 nM)
T allele
C allele (BglI)
Allele T/Allele C
C
DNM2 mRNA (siRNA at 100 nM)
D
BglI digestion (siRNA at 100 nM)
DNM2 protein (siRNA at 100 nM)
E
DNM2
GAPDH
DNM2/GAPDH

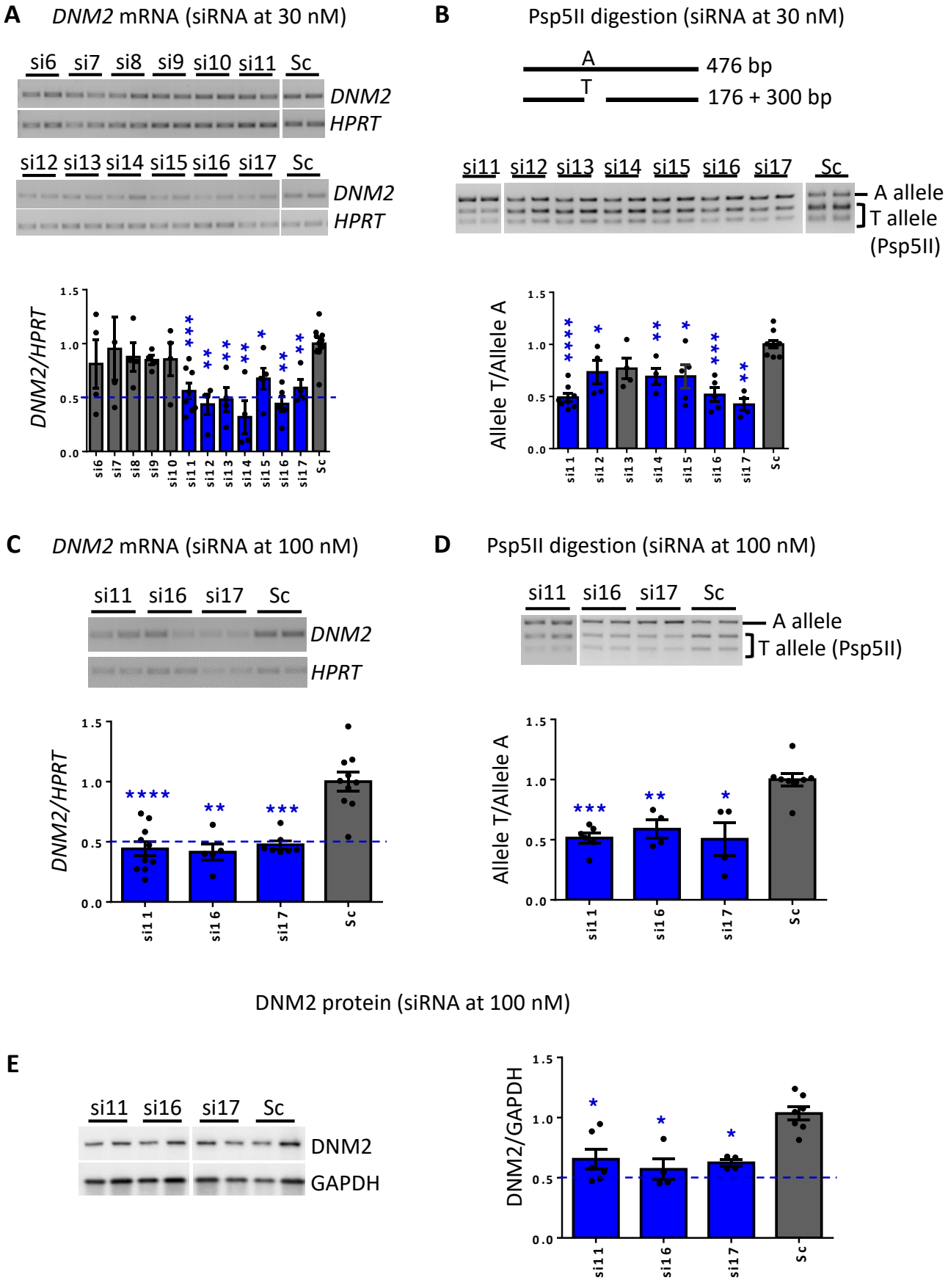
A
DNM2 mRNA (siRNA at 30 nM)
si6 si7 si8 si9 si10 si11 Sc
DNM2
HPRT
si12 si13 si14 si15 si16 si17 Sc
DNM2
HPRT
DNM2/HPRT
B
Psp5II digestion (siRNA at 30 nM)
A
476 bp
T
176 + 300 bp
si11 si12 si13 si14 si15 si16 si17 Sc
A allele
T allele
(Psp5II)
Allele T/Allele A
C
DNM2 mRNA (siRNA at 100 nM)
si11 si16 si17 Sc
DNM2
HPRT
DNM2/HPRT
D
Psp5II digestion (siRNA at 100 nM)
si11 si16 si17 Sc
A allele
T allele (Psp5II)
Allele T/Allele A
DNM2 protein (siRNA at 100 nM)
E
si11 si16 si17 Sc
DNM2
GAPDH
DNM2/GAPDH

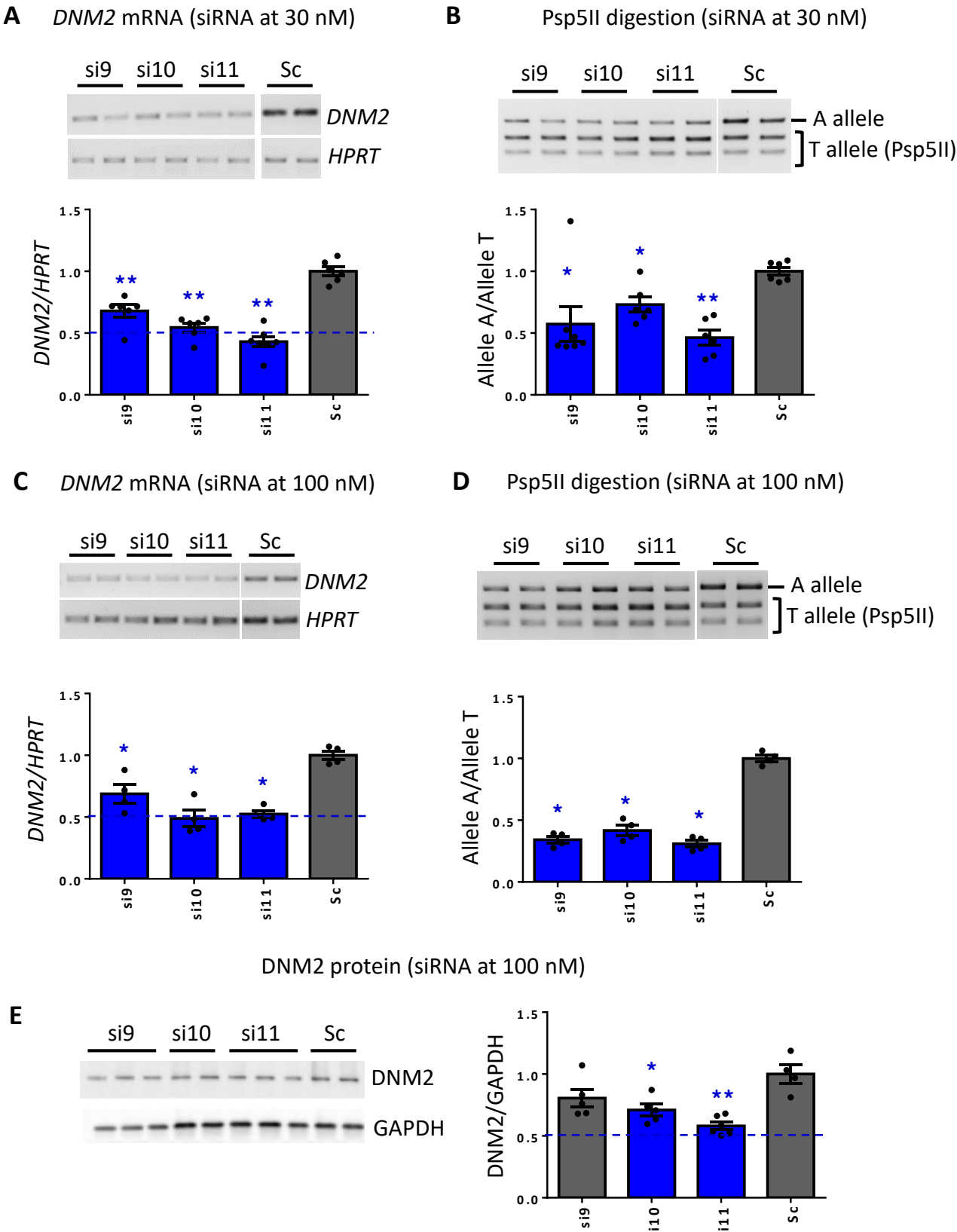
A
DNM2 mRNA (siRNA at 30 nM)
si9
si10
si11
Sc
DNM2
HPRT
DNM2/HPRT
B
Psp5II digestion (siRNA at 30 nM)
A allele
T allele (Psp5II)
Allele A/Allele T
C
DNM2 mRNA (siRNA at 100 nM)
D
Psp5II digestion (siRNA at 100 nM)
DNM2 protein (siRNA at 100 nM)
E
GAPDH
DNM2/GAPDH

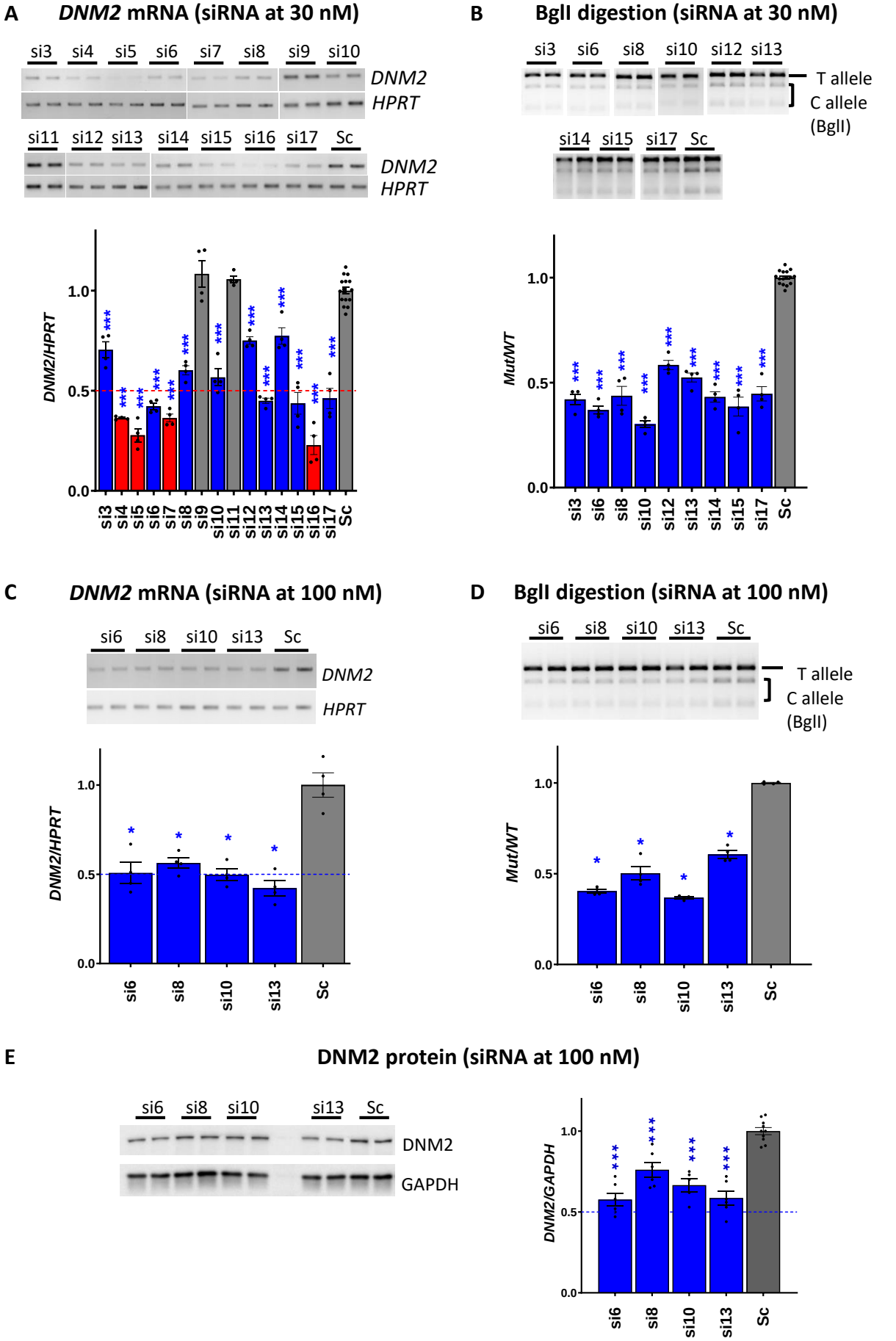
A
DNM2 mRNA (siRNA at 30 nM)
si3 si4 si5 si6 si7 si8 si9 si10
DNM2
HPRT
si11 si12 si13 si14 si15 si16 si17 Sc
DNM2
HPRT
DNM2/HPRT
1.0
0.5
0.0
si3 si4 si5 si6 si7 si8 si9 si10 si11 si12 si13 si14 si15 si16 si17 Sc
B
BglI digestion (siRNA at 30 nM)
si3 si6 si8 si10 si12 si13
si14 si15 si17 Sc
T allele
C allele
(BglI)
Mut/WT
1.0
0.5
0.0
si3 si6 si8 si10 si12 si13 si14 si15 si17 Sc
C
DNM2 mRNA (siRNA at 100 nM)
si6 si8 si10 si13 Sc
DNM2
HPRT
DNM2/HPRT
1.0
0.5
0.0
si6 si8 si10 si13 Sc
D
BglI digestion (siRNA at 100 nM)
si6 si8 si10 si13 Sc
T allele
C allele
(BglI)
Mut/WT
1.0
0.5
0.0
si6 si8 si10 si13 Sc
E
DNM2 protein (siRNA at 100 nM)
si6 si8 si10 si13 Sc
DNM2
GAPDH
DNM2/GAPDH
1.0
0.5
0.0
si6 si8 si10 si13 Sc

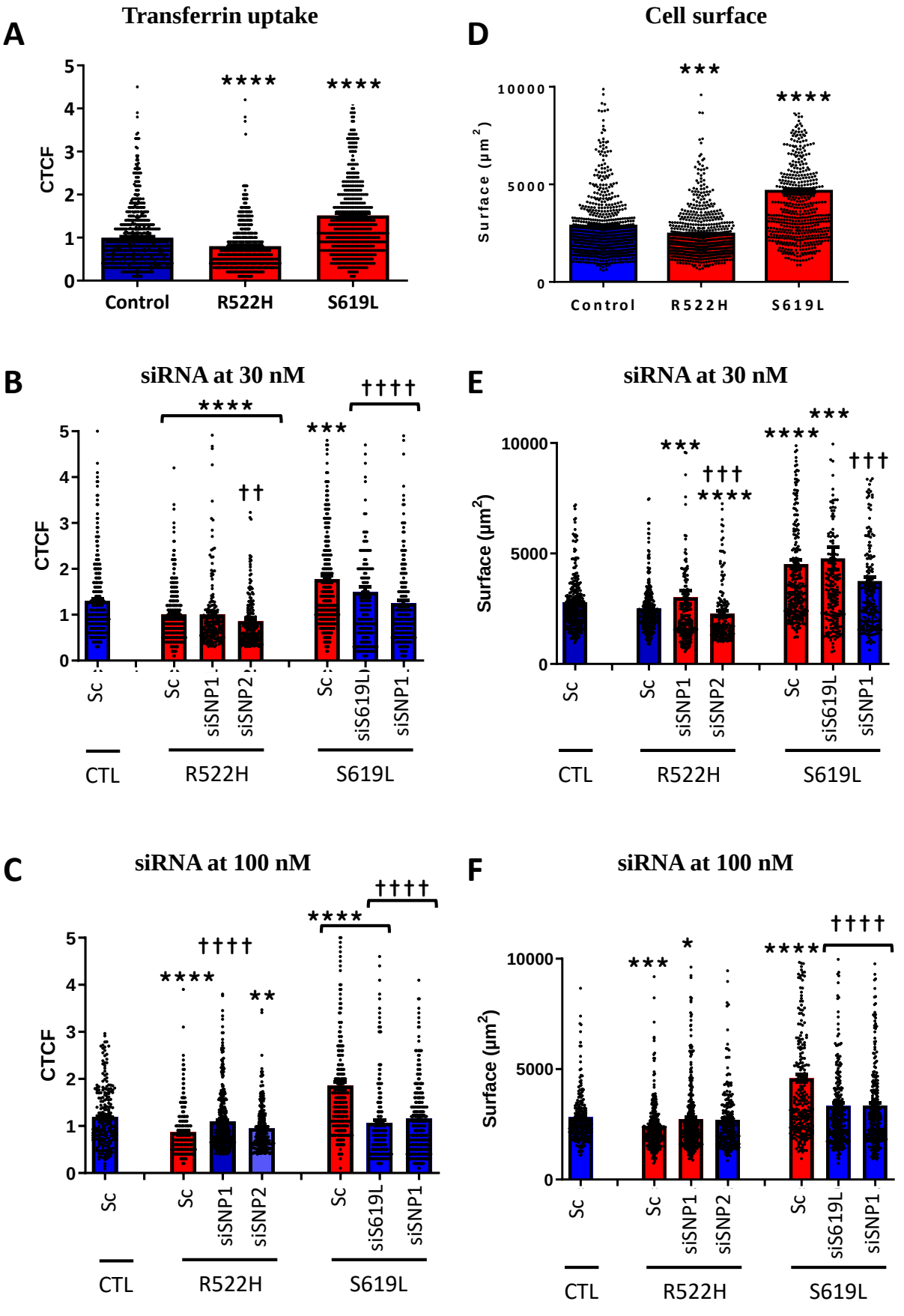
A
Transferrin uptake
CTCF
Control
R522H
S619L
D
Cell surface
Surface (µm²)
B
siRNA at 30 nM
Sc
siSNP1
siSNP2
siS619L
CTL
R522H
S619L
E
C
siRNA at 100 nM
F

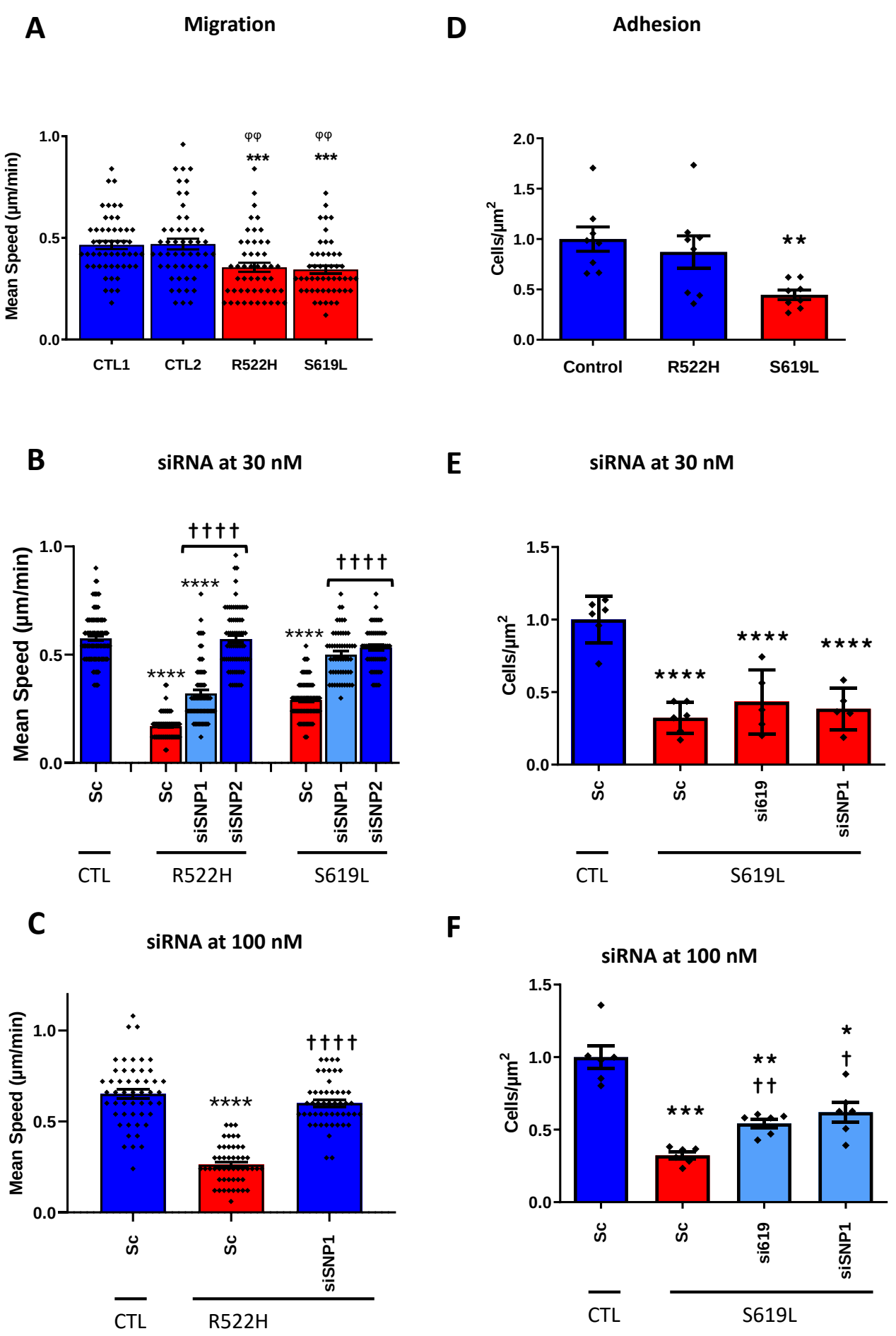
A
Migration
Mean Speed (µm/min)
1.0
0.5
0.0
φφ
***
φφ
***
CTL1
CTL2
R522H
S619L
D
Adhesion
Cells/µm2
2.0
1.5
1.0
0.5
0.0
**
Control
R522H
S619L
B
siRNA at 30 nM
Mean Speed (µm/min)
1.0
0.5
0.0
††††
****
††††
****
****
Sc
Sc
siSNP1
siSNP2
Sc
siSNP1
siSNP2
CTL
R522H
S619L
E
siRNA at 30 nM
Cells/µm2
1.5
1.0
0.5
0.0
****
****
****
Sc
Sc
si619
siSNP1
CTL
S619L
C
siRNA at 100 nM
Mean Speed (µm/min)
1.0
0.5
0.0
****
††††
Sc
Sc
siSNP1
CTL
R522H
F
siRNA at 100 nM
Cells/µm2
1.5
1.0
0.5
0.0
***
**
††
*
†
Sc
Sc
si619
siSNP1
CTL
S619L

Supplementary Figures, Tables and Legends

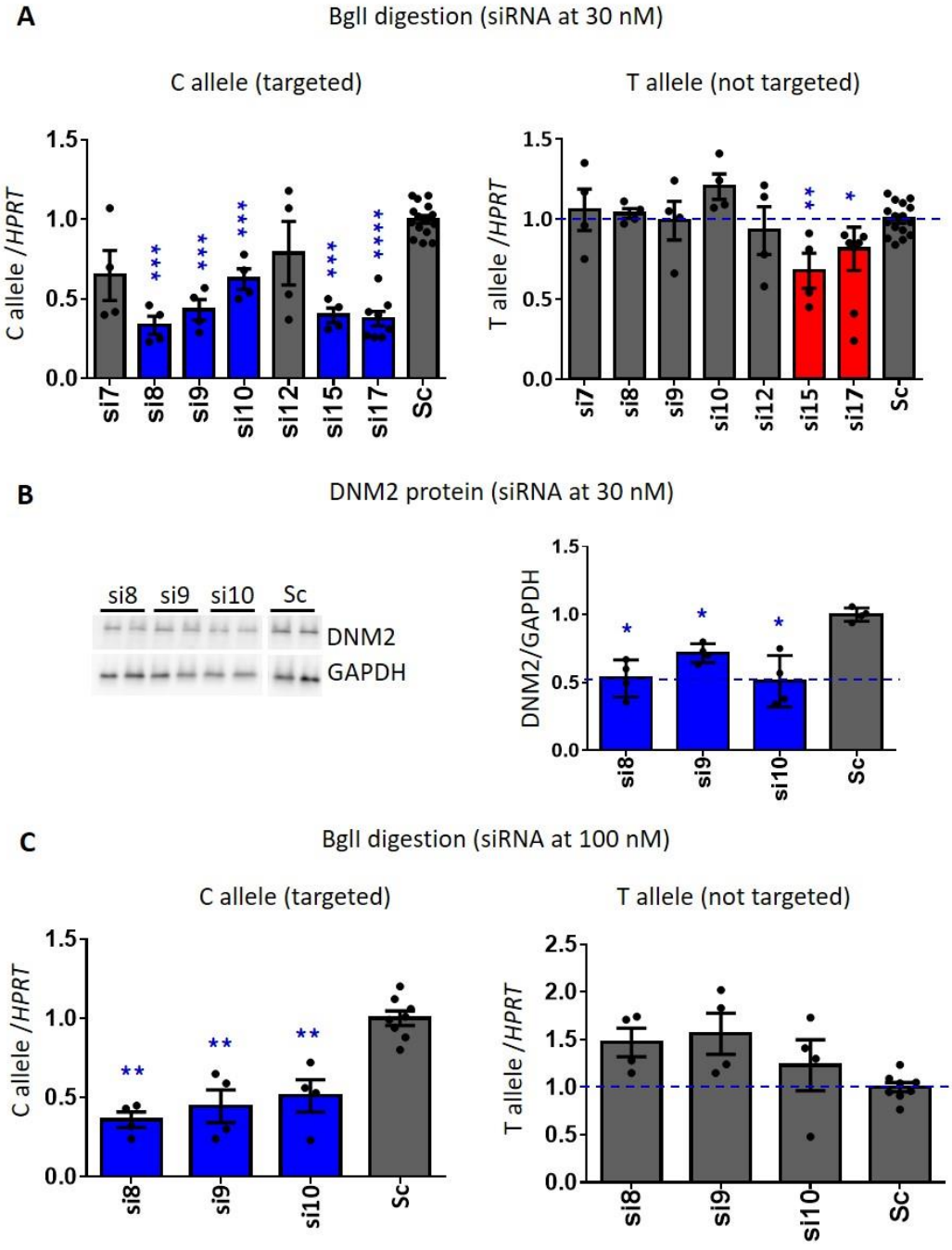

Supplementary Figure 1: Allele-specific siRNA against the C version of SNP1. **A**. Expression of the C and T alleles 48 hours after siRNA transfection at 30 nM. Quantification of the 2 alleles after BglI digestion of the RT-PCR product and normalized to *HPRT* (n ≥4 per condition). **B**. DNM2 western blot and quantification of the signal by densitometry after siRNA

transfection at 30 nM concentration. GAPDH was used as a loading control (n ≥4). **C**. Expression of the C and T alleles 48 hours after siRNA transfection at 100 nM. Quantification of the 2 alleles after BglI digestion of the RT-PCR product and normalized to *HPRT* (n ≥4 per condition). Data information: In scatter plots, the bars are mean values and error bars indicate SEM. ***P < 0.001, **P < 0.01 and *P < 0.5 using a two-tailed Mann–Whitney *U*-test relative to the scramble siRNA (Sc).

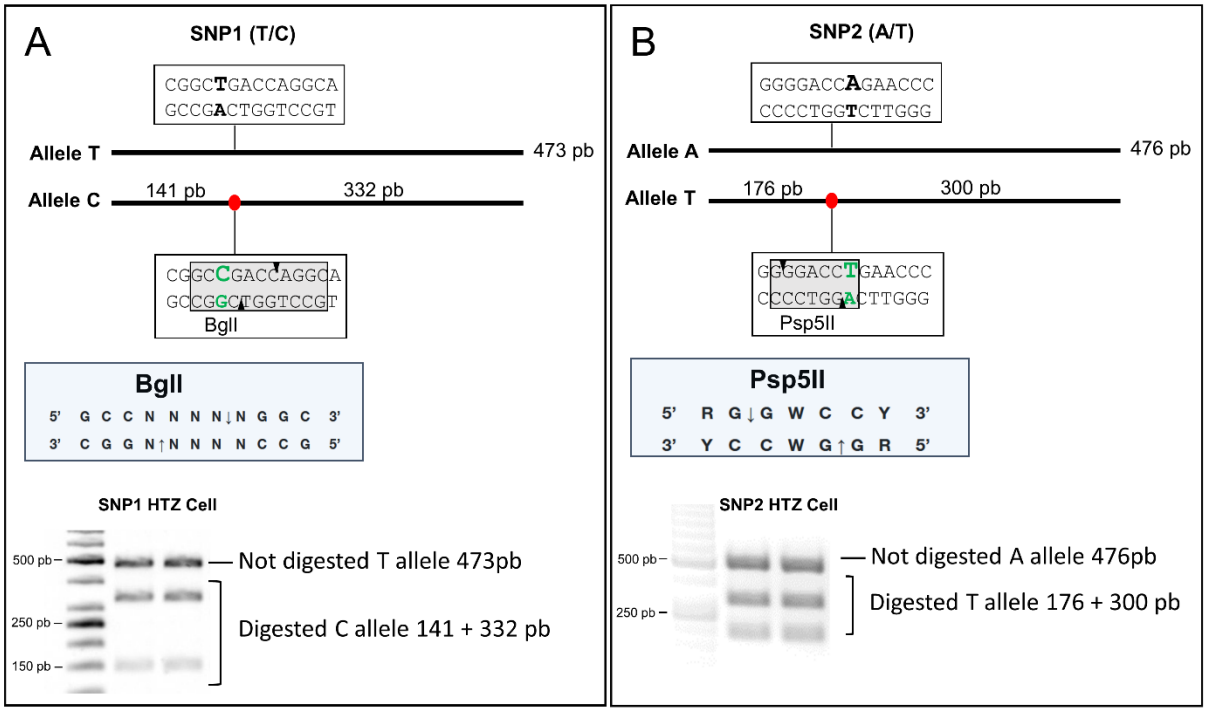

Supplementary Figure 2: RT-PCR assays for identification of SNP allele-specificity in fibroblasts.

Schematic representation of the PCR fragment amplifying the SNP1 (A) and SNP2 (B) regions. The restriction sites used to discriminate the two alleles of each SNP are positioned on the PCR fragments and their nucleotide sequence is shown. The nucleotide variation for each SNP is in bold, in green when the enzyme recognized the site and in black when the recognition is abolished. The size of the digested and undigested PCR amplicons are indicated as well as the canonical recognition sequence for the enzyme BgII and Psp5II. Below, agarose gel electrophoresis of digested PCR amplicons after BglI (left) or Psp5II (right) digestion for cells heterozygous for these SNPs are shown. The enzymatic digestion allows the discrimination between both version of each SNP alleles and quantification of signal associated with both alleles. The associated-signal for the digested allele is obtained by the sum of the signal for the two bands. Length of each band in base-pairs (bp) is indicated on the right.

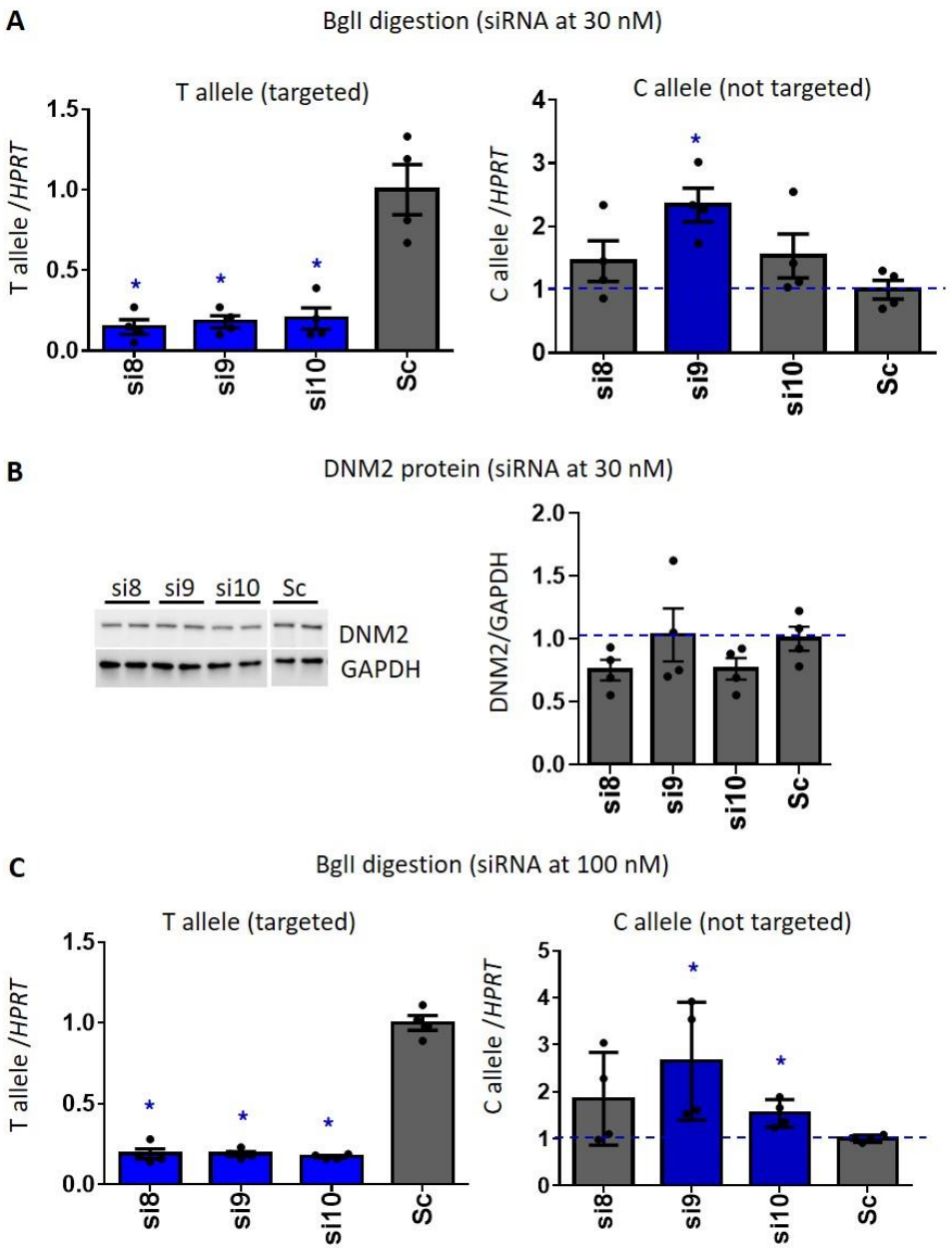

Supplementary Figure 3: Allele-specific siRNA against the T version of SNP1. **A**. Expression of the T and C alleles 48 hours after siRNA transfection at 30 nM. Quantification of the 2 alleles after BglI digestion of the RT-PCR product and normalized to *HPRT* (n ≥4 per condition). **B**. DNM2 western blot and quantification of the signal by densitometry after siRNA transfection at 30 nM concentration. GAPDH was used as a loading control (n ≥4). **C**. Expression of the T and C alleles 48 hours after siRNA transfection at 100 nM. Quantification of the 2 alleles after BglI digestion of the RT-PCR product and normalized to *HPRT* (n ≥4 per

condition). Data information: In scatter plots, the bars are mean values and error bars indicate SEM. *P < 0.5 using a two-tailed Mann–Whitney *U*-test relative to the scramble siRNA (Sc).

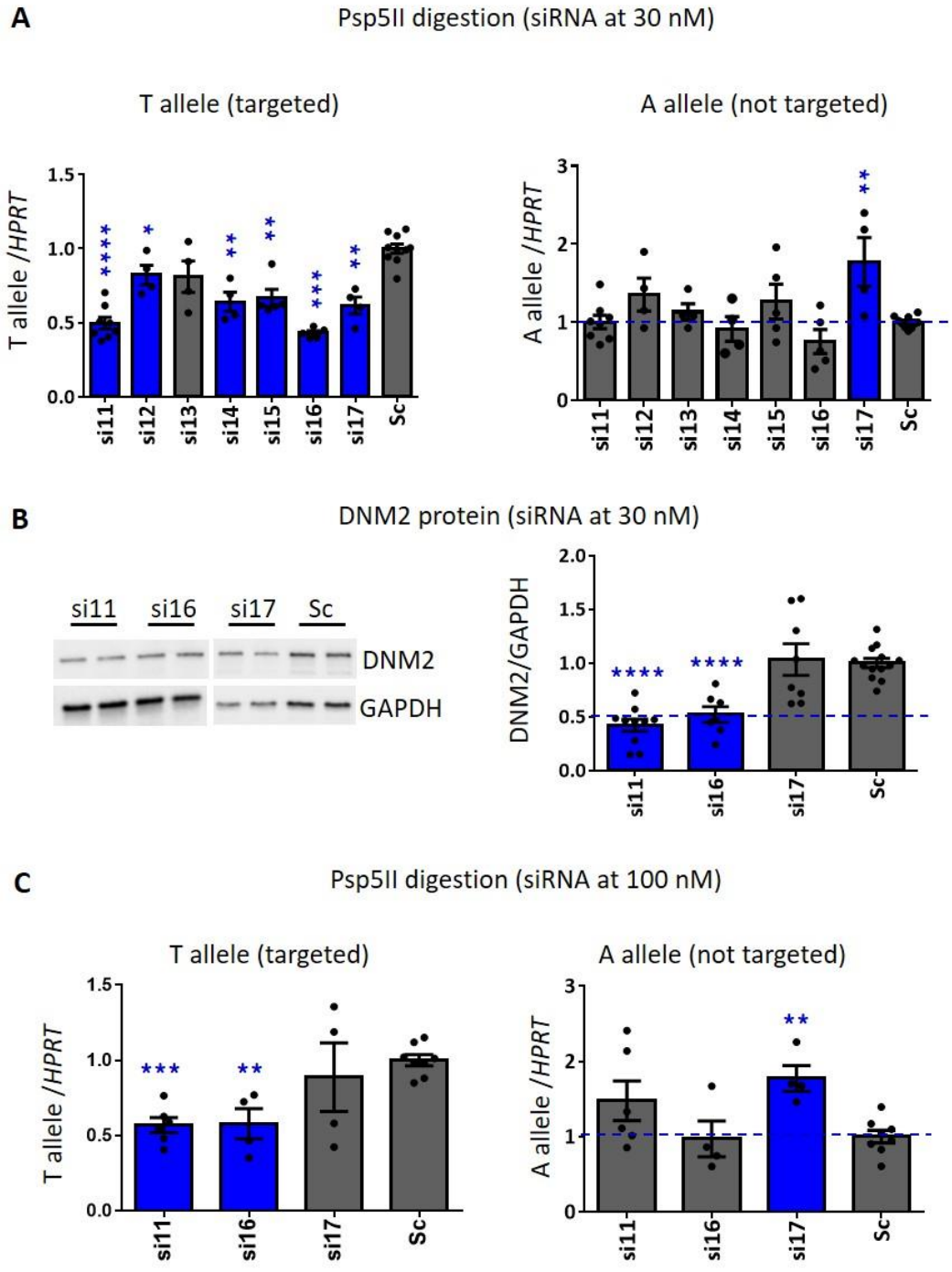

Supplementary Figure 4: Allele-specific siRNA against the T version of SNP2. **A**. Expression of the T and A alleles 48 hours after siRNA transfection at 30 nM. Quantification of the 2 alleles after Psp5II digestion of the RT-PCR product and normalized to *HPRT* (n ≥4 per condition). **B**. DNM2 western blot and quantification of the signal by densitometry after siRNA transfection at 30 nM concentration. GAPDH was used as a loading control (n ≥4). **C**.

Expression of the T and A alleles 48 hours after siRNA transfection at 100 nM. Quantification of the 2 alleles after Psp5II digestion of the RT-PCR product and normalized to *HPRT* ($n \geq 4$ per condition). Data information: In scatter plots, the bars are mean values and error bars indicate SEM. ****$P < 0.0001$, ***$P < 0.001$, **$P < 0.01$ and *$P < 0.5$ using a two-tailed Mann–Whitney *U*-test relative to the scramble siRNA (Sc).

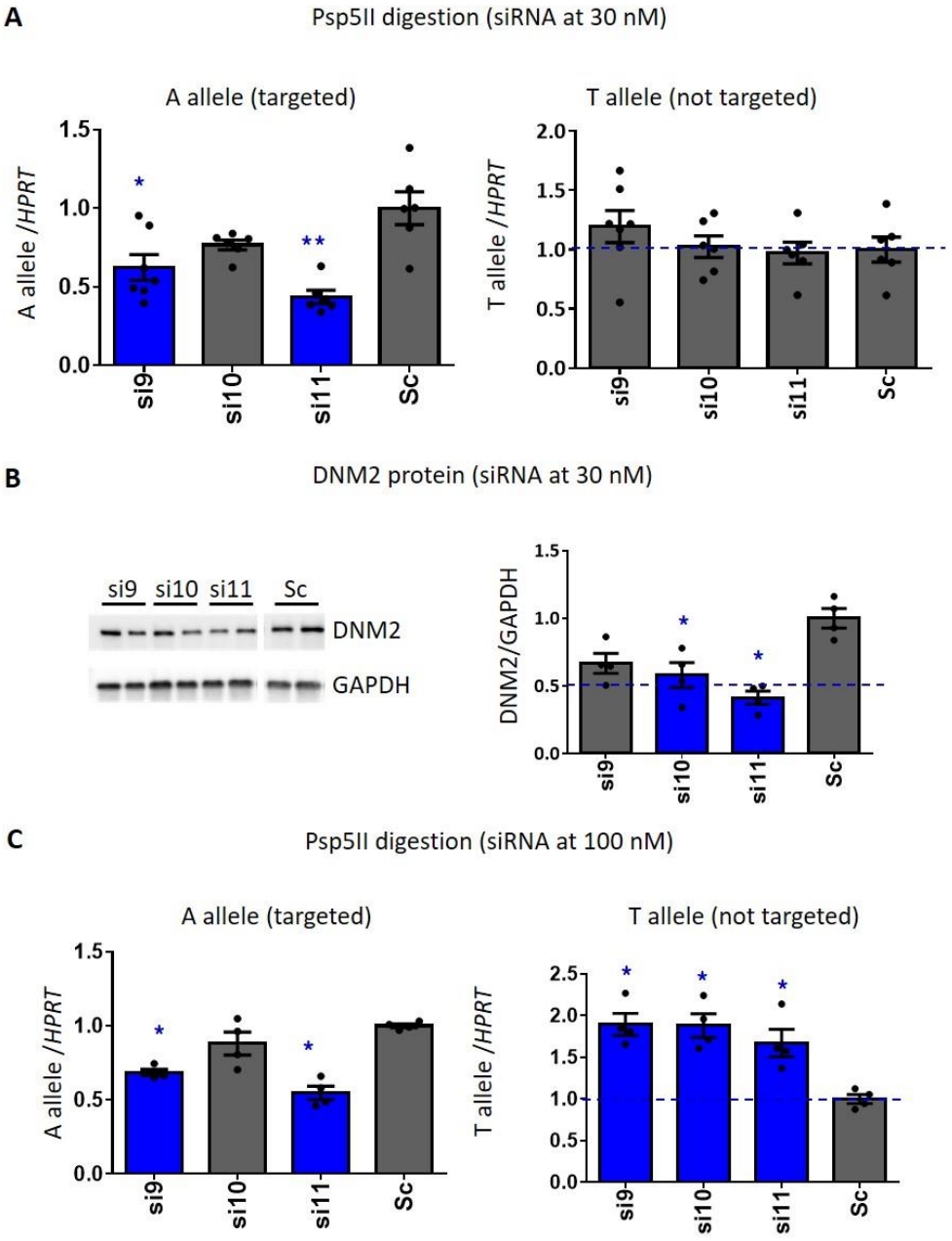

Supplementary Figure 5: Allele-specific siRNA against the A version of SNP2. **A**. Expression of the A and T alleles 48 hours after siRNA transfection at 30 nM. Quantification of the 2 alleles after Psp5II digestion of the RT-PCR product and normalized to *HPRT* (n ≥4 per condition). **B**. DNM2 western blot and quantification of the signal by densitometry after siRNA transfection at 30 nM concentration. GAPDH was used as a loading control (n ≥4). **C**. Expression of the T and A alleles 48 hours after siRNA transfection at 100 nM. Quantification

of the 2 alleles after Psp5II digestion of the RT-PCR product and normalized to *HPRT* ($n \geq 4$ per condition). Data information: In scatter plots, the bars are mean values and error bars indicate SEM. **$P < 0.01$ and *$P < 0.5$ using a two-tailed Mann–Whitney *U*-test relative to the scramble siRNA (Sc).

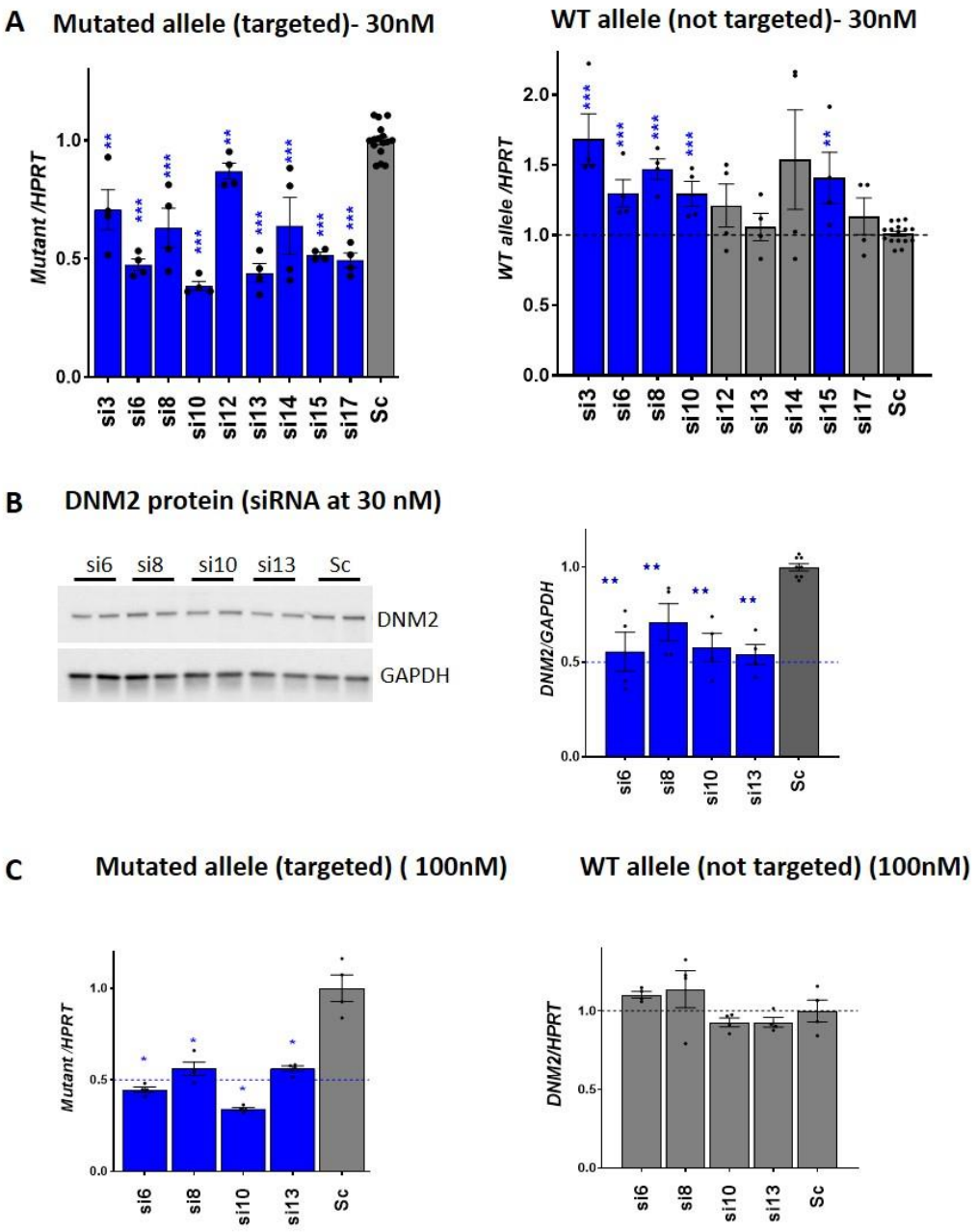

Supplementary Figure 6: Identification of allele-specific siRNA against the S619L mutated allele. **A**. Expression of the mutated and wild-type alleles 48 hours after siRNA transfection at 30 nM. Quantification of the 2 alleles after BglI digestion of the RT-PCR product and normalized to *HPRT* (n ≥4 per condition). **B**. DNM2 western blot and quantification of the signal by densitometry after siRNA transfection at 30 nM concentration. GAPDH was used as a loading control (n ≥4). **C**. Expression of the mutated and wild-type alleles 48 hours after siRNA transfection at 100 nM. Quantification of the 2 alleles after BglI digestion of the RT-

PCR product and normalized to *HPRT* (n ≥4 per condition). Data information: In scatter plots, the bars are mean values and error bars indicate SEM. ***P < 0.001, **P < 0.01 and *P < 0.5 using a two-tailed Mann–Whitney *U*-test relative to the scramble siRNA (Sc).

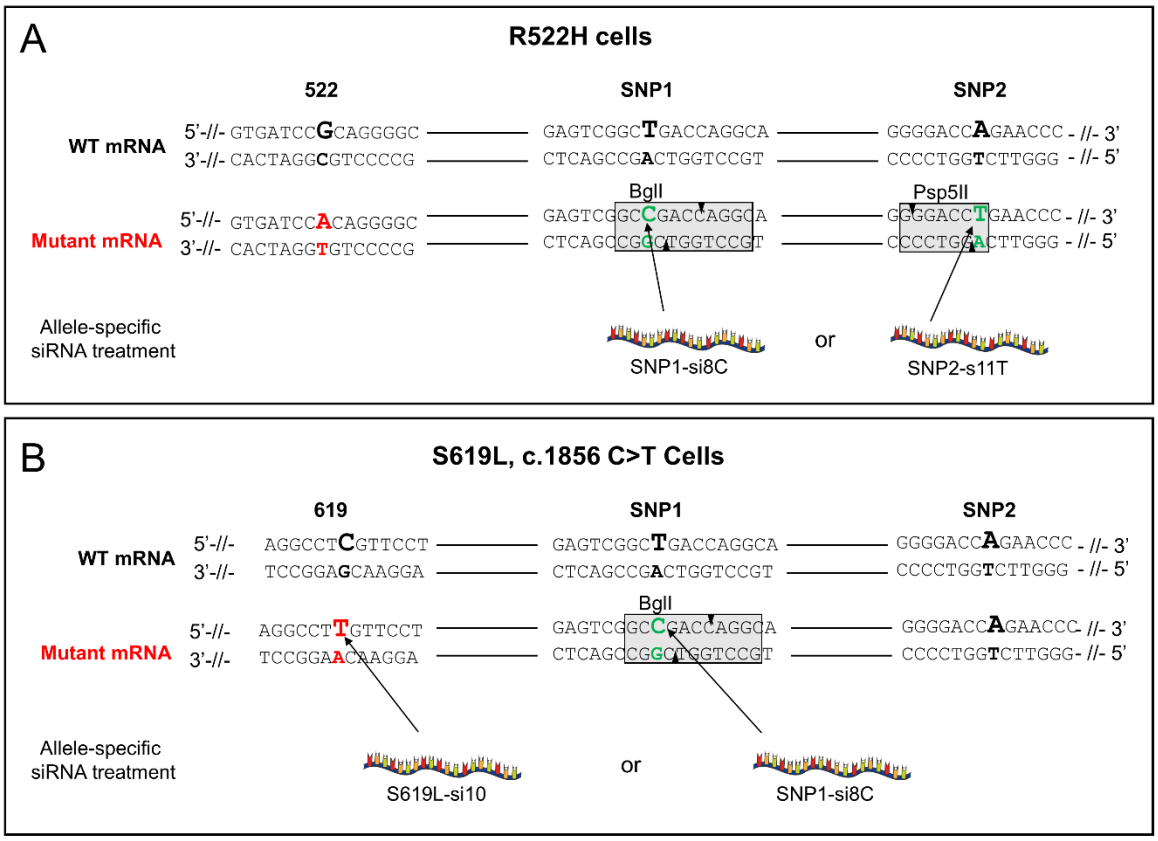

Supplementary Figure 7: Sequences and allelic distribution of DNM2 mutations and SNPs on mRNA from AD-CNM patient's fibroblasts and allele-specific siRNA used for treatment. (A) R522H fibroblasts (B) S619L fibroblasts. For both cell lines, WT and mutant mRNA alleles are depicted showing the sequence of the mutation and the allelic version of the SNP presents on each allele. Allele specific siRNAs used for treatment in each cell lines are shown with their target. The nucleotidic variation for mutations and SNPs is in bold and the nucleotid targeted by the siRNA is in red for the mutation and green for the SNP.

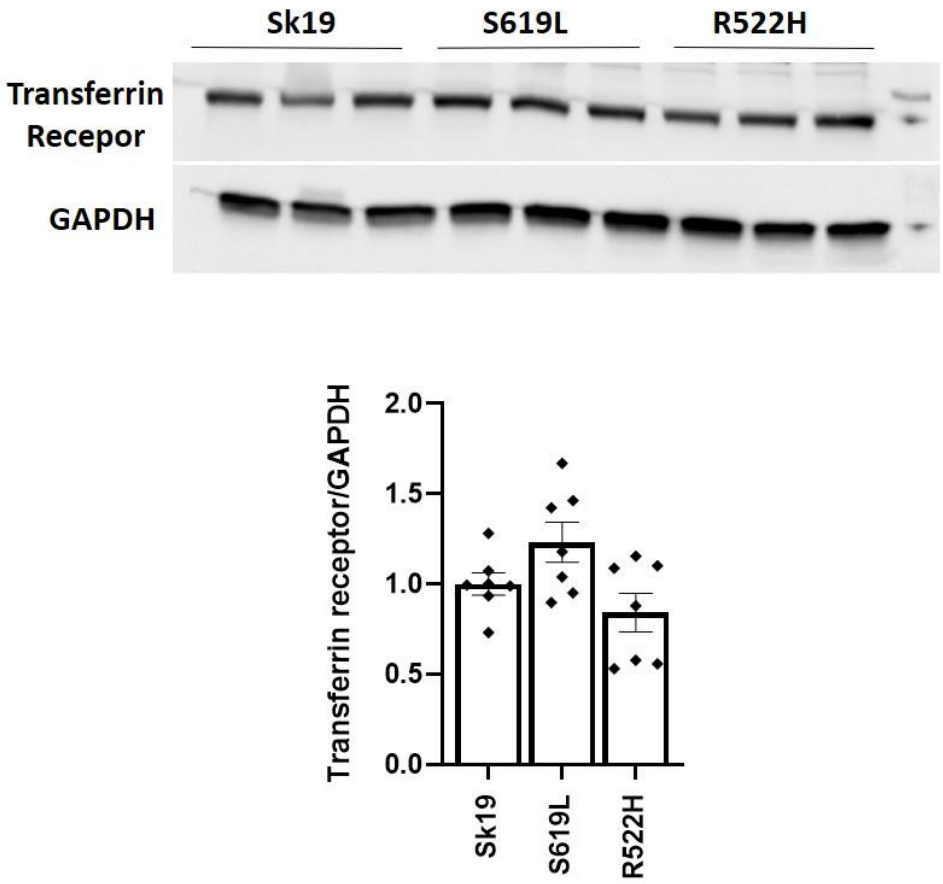

Supplementary Figure 8: Transferrin receptor western blot and quantification of signal by densitometry in control and mutant cells. GAPDH was used as a loading control (n=7). Data information: In scatter plots, the bars are mean values and error bars indicate SEM. Kruskal-Wallis was non-significant.

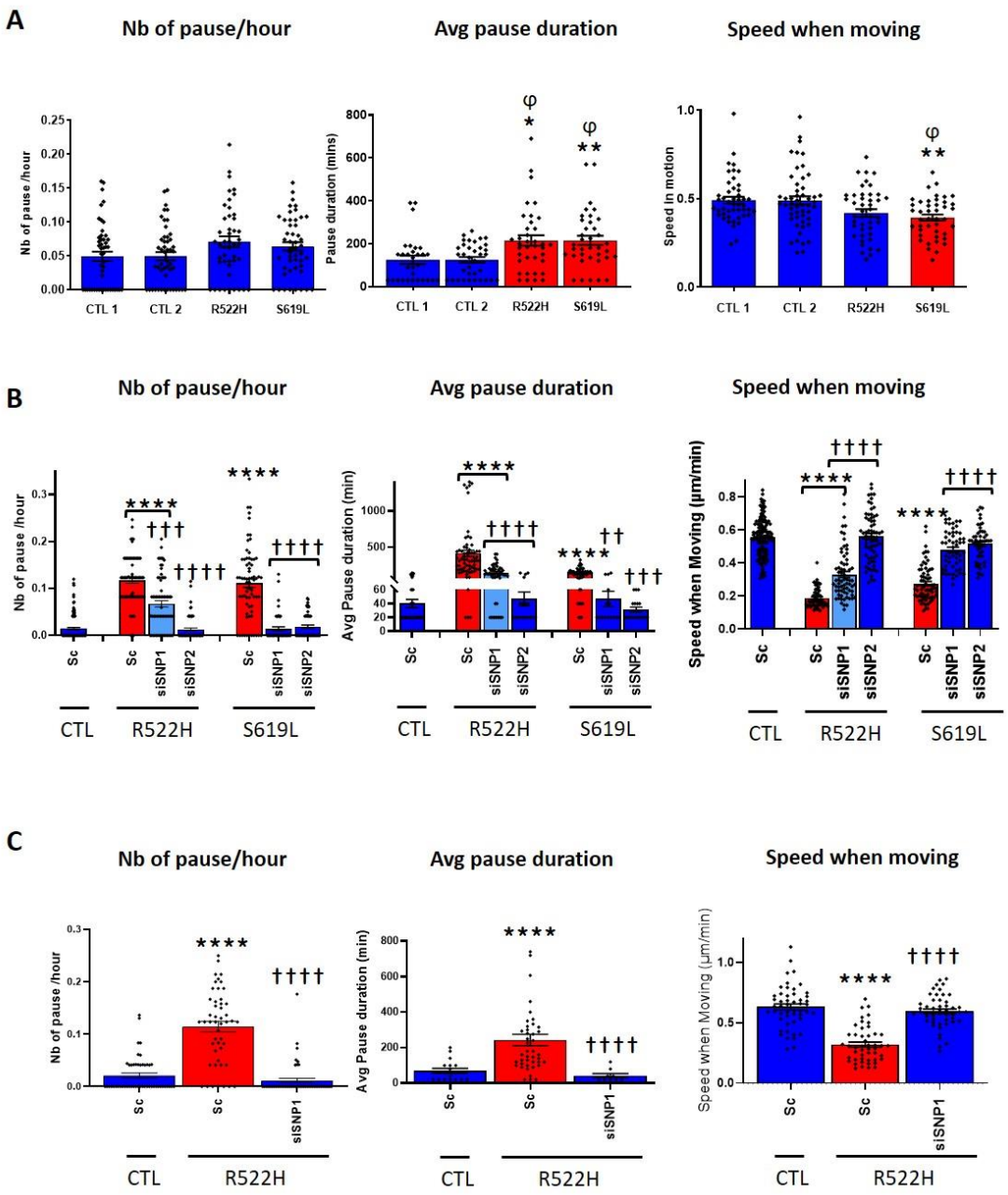

Supplementary Figure 9: **Skypad Analysis of cell motility and maximum speed.** Cell motility analyses were performed using Skypad software, showing the number of pauses per cell per hour tracking, the average duration of pause (in minutes), and the average speed when moving for each cell. All these parameters were plotted for (A) cells under basal conditions, (B) cells 48 hours after transfection at a concentration of 30 nM siRNA and (C) cells 48 hours after transfection at a concentration of 100 nM siRNA. The histograms represent mean ± SEM. Statistical analysis are performed using Kruskal-Wallis, followed by Dunn's test relative to

control cells 1 (** P<0.01, * P<0.05) or control cells 2 (φ P<0.05) in A, or to control cells transfected with scramble siRNA in B and C (**** P<0.0001), or to patient cell lines transfected with scramble siRNA in B and C (†††† P<0.0001, ††† P<0.001, †† P<0.01). Sc: Scramble.

Suplemental Table 1: Mean +/- SEM values for each of the data figures

Figure 2

Figure 2A	si5	si6	si7	si8	si9	si10	si11	si12	si13	si14	si15	si17	Sc
Number of values	4	4	4	4	4	4	4	4	4	4	4	8	16
Mean	0.2325	0.6325	0.6175	0.5525	0.6568	0.502	0.7993	0.6875	0.1575	0.2125	0.6975	0.4564	1,000
SEM	0.03376	0.1924	0.0832	0.06223	0.0843	0.1006	0.1156	0.06115	0.01797	0.01887	0.1256	0.05897	0.0332

Figure 2B	si7	si8	si9	si10	si12	si15	si17	Sc
Number of values	4	4	4	4	4	4	8	16
Mean	0.5225	0.33	0.4325	0.535	0.8075	0.6075	0.5388	1,000
Std. Error of Mean	0.03351	0.06258	0.02869	0.08312	0.0833	0.03092	0.09127	0.01049

Figure 2C	si8	si9	si10	Sc
Number of values	4	4	4	8
Mean	0.4468	0.4095	0.2573	1,000
Std. Error of Mean	0.04338	0.03833	0.02381	0.02677

Figure 2D	si8	si9	si10	Sc
Number of values	4	4	4	8
Mean	0.2415	0.2723	0.426	1,000
Std. Error of Mean	0.0129	0.03026	0.02013	0.02044

Figure 2E	si8	si9	si10	Sc
Number of values	4	4	4	4
Mean	0.525	0.6975	0.57	1,000
Std. Error of Mean	0.08617	0.03351	0.09806	0.02944

Figure 3

Figure 3A	si8	si9	si10	Sc
Number of values	4	4	4	4
Mean	0.4475	0.4975	0.31	1,000
Std. Error of Mean	0.004787	0.0225	0.03764	0.1033

Figure 3B	si8	si9	si10	Sc
Number of values	4	4	4	4
Mean	0.0975	0.075	0.12	1,000
Std. Error of Mean	0.01493	0.00866	0.01472	0.01472

Figure 3C	si8	si9	si10	Sc
Number of values	4	4	4	4
Mean	0.5925	0.5325	0.405	1,000
Std. Error of Mean	0.02562	0.06524	0.02901	0.02041

Figure 3D	si8	si9	si10	Sc
Number of values	4	4	4	4
Mean	0.1175	0.08	0.1175	1,000
Std. Error of Mean	0.01887	0.01472	0.01031	0.01826

Figure 3E	si8	si9	si10	Sc
Number of values	4	4	4	4
Mean	0.6575	0.745	0.625	1,000
Std. Error of Mean	0.04553	0.04787	0.06397	0.0072

Figure 4

Figure 4A	si6	si7	si8	si9	si10	si11	si12	si13	si14	si15	si16	si17	Sc
Number of values	4	4	4	4	4	8	4	4	4	5	5	4	10
Mean	0.8119	0.9516	0.877	0.8476	0.8549	0.5609	0.4369	0.4824	0.3192	0.675	0.4414	0.5906	1,000
Std. Error of Mean	0.2225	0.2927	0.1336	0.04379	0.1502	0.07189	0.09511	0.115	0.1523	0.09761	0.07344	0.07959	0.05327

Figure 4B	si11	si12	si13	si14	si15	si16	si17	Sc
Number of values	8	4	4	4	5	5	4	10
Mean	0.4902	0.7327	0.7687	0.6897	0.6928	0.5171	0.4229	1,000
Std. Error of Mean	0.03832	0.113	0.1	0.07701	0.1114	0.06743	0.05742	0.03475

Figure 4C	si11	si16	si17	Sc
Number of values	10	5	7	10
Mean	0.4415	0.4147	0.4751	1,000
Std. Error of Mean	0.05982	0.06817	0.03278	0.07782

Figure 4D	si11	si16	si17	Sc
Number of values	6	4	4	8
Mean	0.5147	0.5885	0.504	1,000
Std. Error of Mean	0.04336	0.07434	0.136	0.05306

Figure 4E	si11	si16	si17	Sc
Number of values	6	4	4	7
Mean	0.6546	0.5707	0.6243	1.034
Std. Error of Mean	0.08467	0.08649	0.02727	0.05652

Figure 5

Figure 5A	si9	si10	si11	Sc
Number of values	6	6	7	6
Mean	0.6791	0.5452	0.4306	1,000
Std. Error of Mean	0.05002	0.03654	0.04105	0.0371

Figure 5B	si9	si10	si11	Sc
Number of values	7	6	6	6
Mean	0.5729	0.7305	0.4633	1,000
Std. Error of Mean	0.14	0.06196	0.06051	0.03249

Figure 5C	si9	si10	si11	Sc
Number of values	4	4	4	4
Mean	0.6879	0.4889	0.5238	1,000
Std. Error of Mean	0.07457	0.0683	0.02817	0.03623

Figure 5D	si9	si10	si11	Sc
Number of values	4	4	4	4
Mean	0.3413	0.4174	0.3089	1,000
Std. Error of Mean	0.02837	0.04186	0.02852	0.02661

Figure 5E	si9	si10	si11	Sc
Number of values	5	5	6	4
Mean	0.8055	0.709	0.5812	1,000
Std. Error of Mean	0.07197	0.04763	0.03067	0.0779

Figure 6

Figure 6A	si3	si4	si5	si6	si7	si8	si9	si10	si11	si12	si13	si14	si15	si16	si17	Sc
Number of values	4	4	4	4	4	4	4	4	4	4	4	4	4	4	4	16
Mean	0.7047	0.363	0.278	0.4223	0.3638	0.6021	1.084	0.5671	1.057	0.7508	0.4498	0.7734	0.4371	0.2285	0.4614	1,000
Std. Error of Mean	0.03991	0.004007	0.03304	0.01582	0.01962	0.02255	0.06726	0.04148	0.01654	0.01885	0.01325	0.04102	0.05429	0.04761	0.05063	0.01678

Figure 6B	si3	si6	si8	si10	si12	si13	si14	si15	si17	Sc
Number of values	4	4	4	4	4	4	4	4	4	16
Mean	0.42	0.3698	0.4373	0.3013	0.5843	0.5244	0.4319	0.386	0.4471	1,000
Std. Error of Mean	0.02542	0.01877	0.04498	0.01641	0.02175	0.02139	0.02484	0.04506	0.03414	0.008212

Figure 6C	si6	si8	si10	si13	Sc
Number of values	4	4	4	4	4
Mean	0.5075	0.5633	0.4978	0.4223	1,000
Std. Error of Mean	0.05842	0.02949	0.03185	0.04182	0.06843

Figure 6D	si6	si8	si10	si13	Sc
Number of values	4	4	4	4	4
Mean	0.4042	0.5027	0.368	0.6063	1,000
Std. Error of Mean	0.01004	0.03794	0.005713	0.02057	0.003268

Figure 6E	si6	si8	si10	si13	Sc
Number of values	6	6	5	6	10
Mean	0.5767	0.7617	0.666	0.5867	1,000
Std. Error of Mean	0.04072	0.04534	0.04057	0.0424	0.02186

Figure 7

Figure 7A	Control	R522H	S619L
Number of values	717	633	555
Mean	0.997	0.8016	1.516
Std. Error of Mean	0.0295	0.02421	0.04916

Figure 7B	Control-sc	R522H-sc	R522H-siSNP1	R522H-siSNP2	S619L-sc	S619L-si619	S619L-siSNP1
Number of values	304	323	181	202	281	185	212
Mean	1.305	1.008	1.007	0.858	1.777	1.492	1.247
Std. Error of Mean	0.04644	0.03344	0.05922	0.04976	0.07684	0.1135	0.07072

Figure 7C	Control-sc	R522H-sc	R522H-siSNP1	R522H-siSNP2	S619L-sc	S619L-si619	S619L-siSNP1
Number of values	225	303	354	250	272	252	313
Mean	1.194	0.8706	1.098	0.9513	1.859	1.069	1.16
Std. Error of Mean	0.04256	0.02873	0.03455	0.03055	0.07998	0.06344	0.05475

Figure 7D	Control	R522H	S619L
Number of values	717	633	556
Mean	2860	2452	4643
Std. Error of Mean	72.78	53.66	137.7

Figure 7E	Control-sc	R522H-sc	R522H-siSNP1	R522H-siSNP2	S619L-sc	S619L-si619	S619L-siSNP1
Number of values	304	323	207	184	281	187	212
Mean	2793	2501	3014	2283	4523	4776	3757
Std. Error of Mean	79.41	58.68	317.7	112,000	173.4	516.6	188.9

Figure 7F	Control-sc	R522H-sc	R522H-siSNP1	R522H-siSNP2	S619L-sc	S619L-si619	S619L-siSNP1
Number of values	240	303	381	232	272	282	312
Mean	2809	2418	2736	2706	4580	3327	3358
Std. Error of Mean	82.35	63.9	81.81	99.41	176.7	131.7	124.7

Figure 8

Figure 8A	CTL1	CTL2	R522H	S619L
Number of values	52	51	50	50
Mean	0.465	0.4694	0.3552	0.3444
Std. Error of Mean	0.0197	0.02623	0.02234	0.019

Figure 8B	CTL-Sc	R522H-sc	R522H-siSNP1	R522H-siSNP2	S619L-Sc	S619L-siSNP1	S619L-siSNP2
Number of values	139	70	69	70	70	55	53
Mean	0.5758	0.1697	0.3209	0.5717	0.2914	0.5007	0.5343
Std. Error of Mean	0.009245	0.007011	0.01647	0.01682	0.01066	0.01495	0.01296

Figure 8C	CTL-Sc	R522H-Sc	R522H-siSNP1
Number of values	50	50	50
Mean	0.6516	0.2628	0.6
Std. Error of Mean	0.02461	0.01513	0.01814

Figure 8D	Control	R522H	S619L
Number of values	8	8	8
Mean	1,000	0.8723	0.4471
Std. Error of Mean	0.1215	0.1598	0.04734

Figure 8E	CTL-Sc	S619L-Sc	S619L-si619	S619L-siSNP1
Number of values	6	6	5	5
Mean	1,000	0.3227	0.433	0.3858
Std. Error of Mean	0.06563	0.04377	0.0985	0.06423

Figure 8F	CTL-Sc	S619L-Sc	S619L-si619	S619L-siSNP1
Number of values	6	6	6	6
Mean	1,000	0.3229	0.5432	0.6201
Std. Error of Mean	0.07941	0.02367	0.03029	0.06797

Suplemental Table 2: Mean +/- SEM values for each of the data supplemental figures

Figure Sup 1

S1-A-left Pane	si7	si8	si9	si10	si12	si15	si17	Sc
Number of values	4	4	4	4	4	4	8	16
Mean	0.6475	0.335	0.4325	0.625	0.7875	0.3975	0.3763	1,000
Std. Error of Mean	0.1566	0.05635	0.06486	0.06449	0.1988	0.04608	0.04563	0.02451

S1A-Right Panel	si7	si8	si9	si10	si12	si15	si17	Sc
Number of values	4	4	4	4	4	4	8	16
Mean	1.058	1.035	0.99	1.203	0.9275	0.6775	0.8138	1,000
Std. Error of Mean	0.1298	0.03122	0.1209	0.07889	0.1493	0.1089	0.1351	0.02502

S1-B	si8	si9	si10	Sc
Number of values	4	4	4	4
Mean	0.5305	0.716	0.51	1,000
Std. Error of Mean	0.0681	0.0346	0.09443	0.02483

S1-C-left	si8	si9	si10	Sc
Number of values	4	4	4	8
Mean	0.36	0.445	0.51	1,000
Std. Error of Mean	0.04916	0.1025	0.1022	0.04555

S1-C-Right Panel	si8	si9	si10	Sc
Number of values	4	4	4	8
Mean	1.47	1.56	1.23	1,000
Std. Error of Mean	0.1497	0.2151	0.2661	0.04897

Figure Sup 3

S3-A-left	si8	si9	si10	Sc
Number of values	4	4	4	4
Mean	0.1475	0.18	0.2	1,000
Std. Error of Mean	0.04589	0.03764	0.06721	0.1555

S3-A-right	si8	si9	si10	Sc
Number of values	4	4	4	4
Mean	1.453	2.34	1.533	1,000
Std. Error of Mean	0.3194	0.2645	0.3489	0.1495

S3-B	si8	si9	si10	Sc
Number of values	4	4	4	4
Mean	1.453	2.34	1.533	1,000
Std. Error of Mean	0.3194	0.2645	0.3489	0.1495

S3-C-left	si8	si9	si10	Sc
Number of values	4	4	4	4
Mean	0.19	0.19	0.1725	1,000
Std. Error of Mean	0.03109	0.01472	0.0075	0.04564

S3-C-right	si8	si9	si10	Sc
Number of values	4	4	4	4
Mean	1.85	2.65	1.538	1,000
Std. Error of Mean	0.4933	0.6286	0.147	0.03764

Figure Sup 4

S4-A-left	si11	si12	si13	si14	si15	si16	si17	Sc
Number of values	8	4	4	4	5	5	4	10
Mean	0.4966	0.8225	0.8103	0.641	0.6667	0.4293	0.6158	1,000
Std. Error of Mean	0.03955	0.06581	0.1066	0.06474	0.05798	0.0154	0.05759	0.03135

S4-A-right	si11	si12	si13	si14	si15	si16	si17	Sc
Number of values	8	4	4	4	5	5	4	10
Mean	1.002	1.354	1.13	0.9132	1.264	0.7525	1.771	1,000
Std. Error of Mean	0.08623	0.2105	0.1055	0.1582	0.2217	0.1538	0.3127	0.02356

S4-B	si11	si16	si17	Sc
Number of values	10	7	8	13
Mean	0.4206	0.5208	1.032	1,000
Std. Error of Mean	0.05709	0.07277	0.1463	0.04182

S4-C-left	si11	si16	si17	Sc
Number of values	6	4	4	8
Mean	0.5693	0.5779	0.8868	1,000
Std. Error of Mean	0.05066	0.1006	0.2272	0.0367

S4-C-rigth	si11	si16	si17	Sc
Number of values	6	4	4	8
Mean	1.476	0.9704	1.773	1,000
Std. Error of Mean	0.2627	0.2395	0.1695	0.08367

Figure Sup 5

S5-A-left	si9	si10	si11	Sc
Number of values	7	6	6	6
Mean	0.6242	0.7672	0.4372	1,000
Std. Error of Mean	0.08123	0.03147	0.04225	0.1043

S5-A-right	si9	si10	si11	Sc
Number of values	7	6	6	6
Mean	1.194	1.024	0.9713	1,000
Std. Error of Mean	0.1348	0.09105	0.09153	0.1058

S5-B	si9	si10	si11	Sc
Number of values	4	4	4	4
Mean	0.6666	0.5785	0.4123	1,000
Std. Error of Mean	0.07401	0.09336	0.04964	0.07192

S5-C-left	si9	si10	si11	Sc
Number of values	4	4	4	4
Mean	0.6853	0.8798	0.5466	1,000
Std. Error of Mean	0.02085	0.07736	0.04544	0.01306

S5-C-right	si9	si10	si11	Sc
Number of values	4	4	4	4
Mean	1.896	1.881	1.673	1,000
Std. Error of Mean	0.1313	0.1415	0.1647	0.05589

Figure Sup 6

S6-A-left	si3	si6	si8	si10	si12	si13	si14	si15	si17	Sc
Number of values	4	4	4	4	4	4	4	4	4	16
Mean	0.7076	0.4759	0.6316	0.3863	0.8706	0.4412	0.6396	0.5181	0.4948	1,000
Std. Error of Mean	0.08476	0.02392	0.08336	0.01848	0.03363	0.03925	0.1207	0.01135	0.03119	0.01712

S6-A-Rigth	si3	si6	si8	si10	si12	si13	si14	si15	si17	Sc
Number of values	4	4	4	4	4	4	4	4	4	16
Mean	1.683	1.296	1.469	1.293	1.21	1.058	1.538	1.407	1.133	1.01
Std. Error of Mean	0.1801	0.0984	0.07242	0.08906	0.1532	0.09714	0.3552	0.1828	0.1314	0.01745

S6-B	si6	si8	si10	si13	Sc
Number of values	4	4	4	4	8
Mean	0.555	0.71	0.5775	0.54	1,000
Std. Error of Mean	0.1027	0.09823	0.07443	0.05307	0.0188

S6-C-Left	si6	si8	si10	si13	Sc
Number of values	4	4	4	4	4
Mean	0.4457	0.5604	0.3408	0.5611	1,000
Std. Error of Mean	0.01467	0.03664	0.008412	0.01511	0.07281

S6-C-Rigth	si6	si8	si10	si13	Sc
Number of values	4	4	4	4	4
Mean	1.103	1.139	0.9276	0.9281	1,000
Std. Error of Mean	0.02063	0.1184	0.02797	0.03046	0.07003

Figure Sup 8

	Sk19	S619L	R522H
Number of values	7	7	7
Mean	1,000	1.231	0.8408
Std. Error of Mean	0.06192	0.1105	0.1061

Figure Sup 9

S9A

Number of pause /hour	CTL 1	CTL 2	R522H	S619L
Number of values	48	50	46	48
Mean	0.04923	0.04954	0.07087	0.06394
Std. Error of Mean	0.006923	0.005995	0.007839	0.006267

Avg Pause Duration	CTL 1	CTL 2	R522H	S619L
Number of values	30	35	37	37
Mean	124.9	125	214.7	215.2
Std. Error of Mean	19.24	13.16	24.63	21.56

Speed when moving	CTL 1	CTL 2	R522H	S619L
Number of values	47	51	44	43
Mean	0.4921	0.4898	0.4195	0.3934
Std. Error of Mean	0.01908	0.02342	0.02126	0.01709

S9B

Number of pause /hour	Sc	R522H-Sc	R522H-siSNP1	R522H-siSNP2	S619L-Sc	S619L-siSNP1	S619LsiSNP2
Number of values	137	70	69	68	69	52	51
Mean	0.01477	0.1173	0.06735	0.01271	0.1116	0.01448	0.01846
Std. Error of Mean	0.002373	0.006164	0.00677	0.003116	0.009134	0.00408	0.00371

Avg Pause Duration	Sc	R522H-Sc	R522H-siSNP1	R522H-siSNP2	S619L-Sc	S619L-siSNP1	S619LsiSNP2
Number of values	37	68	53	18	57	15	18
Mean	40.27	410.1	143,000	46.67	133.9	46.67	31.11
Std. Error of Mean	5.754	43.51	13.31	10.1	8.693	11.16	3.695

Speed when moving	Sc	R522H-Sc	R522H-siSNP1	R522H-siSNP2	S619L-Sc	S619L-siSNP1	S619LsiSNP2
Number of values	138	63	69	70	68	54	52
Mean	0.5564	0.187	0.3307	0.5611	0.2746	0.4797	0.5144
Std. Error of Mean	0.009777	0.007083	0.01826	0.01816	0.01335	0.01531	0.01477

S9C

Number of pause /hour	Sc	R522H-Sc	R522H-siSNP1
Number of values	50	49	49
Mean	0.02111	0.1146	0.01132
Std. Error of Mean	0.004758	0.009997	0.00447

Avg Pause Duration	Sc	R522H-Sc	R522H-siSNP1
Number of values	18	43	9
Mean	70	243.2	42.22
Std. Error of Mean	13.46	32.41	11.76

Speed whEn moving	Sc	R522H-Sc	R522H-siSNP1
Number of values	50	48	50
Mean	0.6318	0.3191	0.5947
Std. Error of Mean	0.02458	0.02112	0.01896